Aerospace Science and Technology 145 (2024) 108828

Contents lists available at ScienceDirect

Aerospace Science and Technology

journal homepage: www.elsevier.com/locate/aescte

Landing trajectory and control optimization for helicopter encountering different tail rotor pitch lockups

Xufei Yan [a], Ye Yuan [b,*], Renliang Chen [c]

[a] Tianmushan Laboratory, Hangzhou, Zhejiang 311100, China
[b] Department of Aerospace Engineering, Swansea University, Swansea, Wales SA1 8EN, UK
[c] Nanjing University of Aeronautics and Astronautics, Nanjing, Jiangsu 210016, China

ARTICLE INFO

Keywords:
Helicopter
Tail rotor pitch lockup
Flight dynamics model
Optimal control
Autorotation

ABSTRACT

In recent years, tail rotor failure has been a significant factor in helicopter accidents, contributing to around 30 % of all incidents. Among these failures, tail rotor pitch lockup accounts for nearly 2/3. However, there is currently a lack of research on the landing trajectory and control optimization for piloted helicopters facing tail rotor pitch lockup. Therefore, this paper aims to study the landing trajectory and pilot control strategy optimization during helicopter tail rotor pitch lockup. The findings of this research are expected to provide valuable insights and serve as a reference for subsequent real-time pilot-in-the-loop simulations and final flight tests. In this paper, we utilize the UH-60A helicopter as a prototype to establish a flight dynamics model and a pilot model. The aerodynamic forces and induced velocity of the main rotor are calculated using the blade element method and Pitt-Peters model. The rotor flap motion is simplified to a first-order harmonic quantity. We then formulate the problem of safe landing and control optimization as a nonlinear optimal control problem, with the cost function designed to reflect safety and feasibility during the flight and touchdown process. To solve the optimal control problem numerically, we use direct multiple shooting and sequential quadratic programming algorithms. Flight test data for the UH-60A, encompassing steady-state flight, dynamic response, and autorotation landing, are utilized to validate the accuracy of the flight dynamics model and the effectiveness of the optimal control algorithm. Finally, the paper investigates the safe landing trajectories and control strategies for the sample helicopter when encountering high tail rotor pitch lockup and low tail rotor pitch lockup, respectively. Simulation results demonstrate that when the tail rotor is stuck at a high pitch, it is advisable for pilots to execute a high-power state landing by maintaining the engine at high power while reducing forward speed and descent rate. Conversely, when the tail rotor is stuck at a low pitch, flying at an economical speed (in a low-power state) is advantageous, but it does not facilitate a safe landing thereafter. If the pilot attempts a conventional landing, the yaw rate at touchdown would be very high and potentially dangerous. In contrast, if an autorotation landing is executed, the landing will be safer with a much lower yaw rate at touchdown. The optimal landing trajectory and control process align with the recommendations from actual helicopter flight tests. The proposed method provides feasible pilot control strategies for safe landing when helicopters encounter various tail rotor pitch lockup situations. This research can serve as a reference for pilots before conducting actual flight tests.

1. Introduction

Conventional single rotor helicopters rely on a tail rotor to balance the torque generated by the main rotor and to achieve heading control. Consequently, complete or partial tail rotor failure can lead to significant control issues for the helicopter. In recent years, tail rotor malfunctions have been responsible for a substantial proportion of helicopter accidents, accounting for approximately 30 % of all incidents [1–3]. Helicopter tail rotor failures can be classified into three main types: aerodynamic failures, complete tail rotor system failures, and tail rotor pitch lockups. Aerodynamic failure occurs when the tail rotor is unable to function properly due to vortex ring, resulting in a loss of tail rotor effectiveness. In such cases, the pilot can mitigate the issue by accelerating the helicopter forward to dissipate the vortex ring at the tail rotor using the airflow. This type of failure is generally straightforward to avoid or resolve. Complete tail rotor failure refers to the situation where the tail rotor fails to generate lateral force. This failure can result

* Corresponding author.
E-mail address: ye.yuan@swansea.ac.uk (Y. Yuan).

https://doi.org/10.1016/j.ast.2023.108828
Received 21 August 2023; Received in revised form 3 December 2023; Accepted 12 December 2023
Available online 16 December 2023

Nomenclature

a	slope of the rotor blade lift curve
a_0, a_1, b_1	taper, rear, and side angles of the rotor disk, rad
b	number of rotor blades
c	blade segment chord length, m
C_T, C_{TR}	rotor thrust coefficient; tail rotor thrust coefficient
$\boldsymbol{D}$	damping matrix
e	flapping hinge offset, m
f_G	ground effect factor
$\boldsymbol{f}$	extrinsic motivator vector
g	acceleration of gravity, m/s^2
h	height, m
H_W	rotor drag force in wind axis, N
H_p	transfer function of pilot model
I_x I_y I_z	inertias of helicopter, kg·m^2
I_{MR},I_{TR}	rotational inertias of the main rotor and tail rotor, kg·m^2
I_β	inertia moment of blade flapping, kg·m^2
J	performance index
k_T	ratio of tail rotor speed to main rotor speed
k_x, k_v	scaling factors
K_β	equivalent flapping torsion spring stiffness, N·m/rad
$\boldsymbol{K}$	stiffness matrix
m_b	mass of the blade, kg
M_β	mass moment of blade flapping, kg·m
M_W, L_W	rotor pitch and roll hub moments, N·m
N	number of nodes
P_A,P_{MR},P_{TR}, P_R	engine output power; required power of the main rotor; required power of the tail rotor; power required by the helicopter, kW
p,q,r	angular velocities of the body axis system, rad/s
p_{HW}, q_{HW}	hub roll and pitch angular velocities under the rotor wind axis system, rad/s
Q	rotor torque, N·m
R	rotor radius, m
r'	radial length from the blade profile to the flapping hinge, m
t	time, s
t_d, t_0, t_f	delay time, initial time, and final time, s
T_L, T_I, T_N	feedforward time constant, inertia time constant, lag time constant, s
$\overline{U}_T$, $\overline{U}_P$	blade profile normalized tangential and normal airflow velocities
$\boldsymbol{u}_b$, $\boldsymbol{u}_d$, $\boldsymbol{u}_f$	control stick vector, delayed command input vector, final control input vector
$\boldsymbol{u}$	control vector (the first-order derivative of the control inputs)
$\mathbf{u}_{delay}$	control vector at t_d
u_{col}, u_{lon}	rate of collective pitch input, longitudinal stick input, and lateral stick input, %/s
u,v,w	linear velocities of the aircraft body axis system, m/s
u_e, v_e, w_e	ground-axis forward velocity, lateral velocity, and descent rate, m/s
w_b, w_v, w_u, w_a	weighting factors in the performance index
$\mathbf{x}_F, \mathbf{x}_R, \mathbf{x}_I$	fuselage motion state vector, rotor flapping state vector and rotor inflow state vector
$\boldsymbol{x}$	state vector
$\mathbf{x}_{delay}$	state vector at t_d
$\boldsymbol{x}_p$	relevant state variables of the neuromuscular system
$\mathbf{X}$	discrete optimal variables
$\widehat{\mathbf{x}}_{k+1}$	The shooting of discrete time segment k
x,y	longitudinal, lateral position in inertial frame, m
Y_W	lateral force in wind axis, N
z	height of the rotor hub above the ground, m
β	blade flapping angle, rad
β_{sp}	helicopter's body slip angle, rad
δ	drag coefficient of the blade airfoil
δ_{col},δ_{lon},δ_{lat},δ_{ped}	collective stick input, longitudinal stick input, lateral stick input, and pedal input, %
η	power transmission coefficient
θ	pitch angle, rad
θ_G	blade profile pitch angle, rad
κ	rotor tip loss coefficient
λ, λ_{TR}	inflow ratio of rotor; inflow ratio of tail rotor
μ, μ_{TR}	advance ratio of the rotor; advance ratio of tail rotor
$\nu_0, \nu_{1s}, \nu_{1c}$	rotor uniform inflow, first-order sine inflow, and first-order cosine inflow
ν_{0T}	uniform inflow of tail rotor
ρ	local atmospheric density, kg/m^3
σ	rotor solidity
τ	non-dimensional time
τ_p	delay time of delay element in the pilot model, s
φ	roll angle, rad
φ'	blade azimuth angle, rad
ψ	yaw angle, rad
Ω	main rotor speed, rad/s

in significant deflection of the fuselage at high yaw angular velocities, especially at low to medium speeds. In such scenarios, it is recommended that the pilot immediately perform an autorotation landing [4,5]. Tail rotor pitch lockup refers to a situation where the tail rotor pitch control mechanism becomes stuck at a particular value and cannot be adjusted. This condition is known as a frozen control state, where any change in power, speed, or sideslip angle can cause directional imbalance. Statistical data shows that tail rotor pitch lockup is the most common type of tail rotor failure, accounting for approximately 2/3 of all failures [2–4].

In recent years, significant research has been conducted to address the issue of helicopter tail rotor pitch lockup. Ref. [6] focused on developing a predictive health management (PHM) system for both the main and tail rotor actuators. The researchers proposed a particle filtering method to predict faults in these actuators. Ref. [7] studied the causes and mechanisms of fatigue failure in helicopter tail rotor blade beams during flight. Ref. [8] introduced the operational modal analysis (OMA) method, which can be used for permanent monitoring of the tail rotor structure. Ref. [9] combined physics-based simulation results with machine learning techniques to establish a parameter substitution model for detecting the proximity of loss of tail rotor effectiveness (LTE) events. Refs. [4,10] mainly carried out landing flight tests for low pitch lockup, and gave basic operation suggestions for different levels of tail rotor pitch lockup. Ref. [11] proposed a method that can simulate tail rotor drive failures during flight testing and provided the corresponding corrective measures. Ref. [12] designed a multi-loop PID controller to ensure the safe flight of unmanned helicopters after tail rotor failure in hovering state. Ref. [13] discussed the different tail rotor failures encountered by the helicopter during flight, and conducted pilot-in-the-loop flight simulation to retrim it under specific flight conditions. Based on the above research, it seems that there is currently a lack of research on the landing trajectory and control optimization for piloted helicopters facing tail rotor pitch lockup. Therefore, this paper aims to study the landing trajectory and pilot control strategy

Table 1
Basic parameters of UH-60A [23].

Parameter	Value
Gross mass (kg)	7257
Number of blades of main rotor	4
Main rotor speed (rad/s)	27
Main rotor radius (m)	8.1778
Main rotor shaft tilt (deg)	3
Flapping hinge offset (m)	0.381
Tail rotor radius (m)	1.6764
Number of blades of tail rotor	4
Inertia I_x I_y I_z (kg·m^2)	5466.9, 39,500, 36,917
Main rotor inertia (kg·m^2)	9569.5
Main rotor solidity	0.0826
Engine response time (s)	1.5
Power transmission coefficient η	0.9
Horizontal tail aerodynamic reference area (m^2)	4.18
Horizontal tail incidence angle (deg)	0
Vertical tail aerodynamic reference tail area (m^2)	3

optimization during helicopter tail rotor pitch lockup. The findings of this research are expected to provide valuable insights and serve as a reference for subsequent real-time pilot-in-the-loop simulations and final flight tests, contributing to the optimization and refinement of control system design.

Numerous scholars have conducted research on flight path, trajectory, and control optimization for aircraft, achieving relatively mature results that greatly inspire the study of landing trajectory and control optimization for piloted helicopters facing tail rotor pitch lockup. Ref. [14] focused on the effective control of a three-axis gimbal system mounted on a UAV for improved real-time target tracking performance under external disturbances. The study contributes to the development of a mathematical model, linear and nonlinear modeling, and the successful implementation of the MPC algorithm, ensuring precise target tracking and system stability even with external disturbances. Ref. [15] focused on real-time control of a UAV using a neural network to ensure precise payload delivery to targets along a specified path. A UAV's Nonlinear Autoregressive exogenous (NARX) model was developed for real-time path tracking. A Load Transporting System (LTS) was designed to transport and deliver payloads to targets while considering environmental limitations and path tracking. The study examined the impact of these factors on the NARX control algorithm's mission performance. Ref. [16] focused on optimizing the attitude and altitude control of UAVs for accurate path following using metaheuristic optimization algorithms based on swarm intelligence, such as Particle Swarm Optimization (PSO) and Harris Hawks Optimization (HHO). A new control algorithm with optimized PID parameter values was proposed for UAV's attitude and altitude control, offering advantages such as simplicity, flexibility, random search ability, and avoidance of local optima. The performance of various control algorithms was tested and compared on specified routes with different geometries. Ref. [17] addressed the growing interest in using drones for various applications while considering the risks associated with emergency scenarios, such as motor failure. The proposed design involved breaking safety requirements into functional and physical requirements, and creating functional and physical architectures for drones. The design suggests drones aggregate their environmental perception through a "potential landmark databank" to maximize the safety of people and assets in emergency situations. Ref. [18] presented a novel hybrid form of Dubins-simulated annealing (HDSA) optimization framework for emergency landing of impaired airplanes with degraded performance characteristics. The HDSA framework generates candidate trajectories considering post-failure performance and environmental constraints, and selects the optimal trajectory to guide the airplane to the desired landing site. The effectiveness of the proposed approach was demonstrated through simulations, aiming to enhance flight management systems and assist pilots in planning suitable emergency landing trajectories. Ref. [19] proposed a safe emergency landing approach for autonomous rotorcrafts in 3D terrains. It combines trajectory optimization and path planning for obstacle-free flight, with an Incremental Backstepping controller for trajectory tracking. Simulations showed the method's effectiveness in ensuring rotorcraft safety during emergency landings like engine failure. Ref. [20] analyzed the impact of variable rotor speed on the low-speed H-V diagram of a UH-60A helicopter in one engine inoperative (OEI) situations by validating a flight dynamics model and applying optimal control methods against flight test data. Ref. [21] developed an augmented longitudinal rigid-body model for the landing procedure of XV-15 tilt-rotor aircraft in single-engine failure scenarios by formulating it as a nonlinear optimal control problem, incorporating pilot inherent limitations. Ref. [22] presented a method to predict pilot workload during helicopter landing using a nonlinear optimal control approach, with results showing consistency between the proposed method and flight test data.

According to the research described above, these studies share a common focus on enhancing the flight performance and safety of helicopters or UAVs in various scenarios. They achieve this through the development and application of advanced control algorithms, optimization methods, and flight dynamics models, offering both theoretical foundations and practical guidance for addressing real-world flight challenges. In comparison, this paper specifically concentrates on the investigation of safe landing control strategies for piloted helicopters encountering tail rotor pitch lockup issues. To tackle this problem effectively, this paper aims to establish a more accurate nonlinear flight dynamics model and pilot model to provide a more precise representation of helicopter dynamics and pilot behavior.

Tail rotor pitch lockup in helicopter can be classified into two common cases, namely high pitch lockup and low pitch lockup. When encountering high tail rotor pitch lockup, the helicopter is generally in a state of high power or low forward speed. On the other hand, when encountering low tail rotor pitch lockup, the helicopter is generally in a state of low power or economic speed. Consequently, the landing trajectories and control strategies corresponding to the two situations will also be different. Therefore, this paper studies the optimal safe landing process of a helicopter encountering high and low tail rotor pitch lockups, respectively. The problem of achieving a safe landing for a helicopter experiencing tail rotor pitch lockup can be described as an underactuated control optimization problem. This type of problem is typically addressed using optimal control method, which is commonly employed to calculate and analyze the optimal flight trajectory and control strategy for helicopters in the case of engine failure, providing valuable guidance and a foundation for conducting flight tests [19–22]. Therefore, this paper investigates the landing trajectory and control optimization for helicopters encountering various tail rotor pitch lockup scenarios using an optimal control method.

The structure of this paper is organized as follows: Section 2 presents the development of a comprehensive flight dynamics model for a single rotor helicopter (UH-60A) with a tail rotor. In Section 3, the problem of optimal safe landing and control is formulated as a nonlinear optimal control problem, considering a pilot model. The problem is then solved numerically using direct multiple shooting and sequential quadratic programming (SQP) algorithms. In Sections 4 and 5, we investigate the scenarios of high and low tail rotor pitch lockup, respectively. For the case of low tail rotor pitch lockup, we also examine the safety implications of employing conventional landing and autorotation landing techniques during the landing phase. Finally, Section 6 presents the conclusions of this study, summarizing the findings and contributions of this research.

2. Flight dynamics modeling and validation

2.1. Flight dynamics modeling

Firstly, this paper utilizes the UH-60A as a prototype to establish a

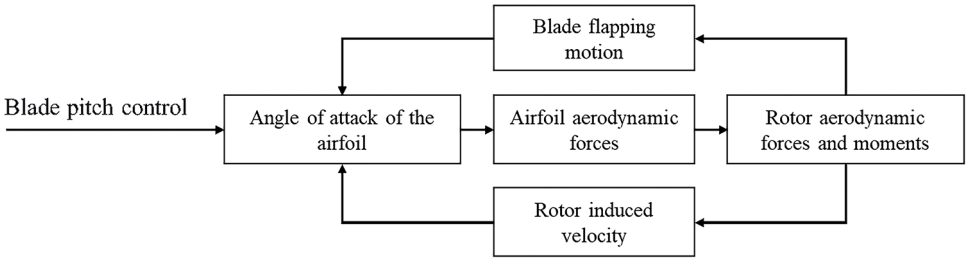

Fig. 1. Helicopter rotor aerodynamic characteristics.

flight dynamics model. The basic parameters of the UH-60A prototype are shown in Table 1 [23].

It is a high-order nonlinear flight dynamics model consisting of a main rotor, a tail rotor and an airframe with vertical tail and horizontal tail. A brief introduction to the model is provided below.

1. The aerodynamic forces and moments acting on the main rotor are calculated using the blade element method. Lift, drag, and moment are determined for each blade element using a table lookup method, which considers flow separation and transonic compressibility effects. The induced velocity is described using the first-order dynamic inflow model proposed by Pitt-Peters [24]. (Fig. 1)

The expressions for rotor thrust, drag, and lateral force are:

$$\begin{cases} T = \sum_{i=1}^{b} \kappa \int_0^{R-e} F^1(\varphi_i')dr' - b\left[M_\beta \ddot{a}_0 + m_b g - m_b(\dot{w} - uq + pv)\right] \\ H_W = \sum_{i=1}^{b} \int_0^{R-e} F^3(\varphi_i')\sin\varphi_i' dr' - \kappa \int_0^{R-e} \left(F^2(\varphi_i')\sin\varphi_i' + F^1(\varphi_i')\beta_i \cos\varphi_i'\right)dr' \\ Y_W = \sum_{i=1}^{b} - \int_0^{R-e} F^3(\varphi_i')\cos\varphi_i' dr' + \kappa \int_0^{R-e} \left(F^2(\varphi_i')\cos\varphi_i' - F^1(\varphi_i')\beta_i \sin\varphi_i'\right)dr' \end{cases} \tag{1}$$

$$\begin{cases} F^1(\varphi_i') = \frac{1}{2}\rho ac(\Omega R)^2\left(\overline{U}_T^2\theta_G + \overline{U}_T\overline{U}_P\right) \\ F^2(\varphi_i') = \frac{1}{2}\rho ac(\Omega R)^2\left(\overline{U}_T\overline{U}_P\theta_G + \overline{U}_P^2\right) \\ F^3(\varphi_i') = \frac{1}{2}\rho c(\Omega R)^2\delta\overline{U}_T^2 \end{cases} \tag{2}$$

The rotor torque is represented as:

$$Q = \sum_{i=1}^{b} \int_0^{R-e} (e + r')F^3(\varphi_i')dr' - \kappa \int_0^{R-e} (e + r')F^2(\varphi_i')dr' + I_{MR}\dot{\Omega} \tag{3}$$

The rotor pitch and roll hub moments are represented as:

$$\begin{cases} M_W = \sum_{i=1}^{b} -\kappa \int_0^{R-e} eF^1(\varphi_i')\cos\varphi_i' dr' + \left(eM_\beta \ddot{\beta}_i - K_\beta\beta_i\right)\cos\varphi_i' \\ L_W = \sum_{i=1}^{b} -\kappa \int_0^{R-e} eF^1(\varphi_i')\sin\varphi_i' dr' + \left(eM_\beta \ddot{\beta}_i - K_\beta\beta_i\right)\sin\varphi_i' \end{cases} \tag{4}$$

Where ρ denotes the local atmospheric density; a denotes the blade lift line slope; b denotes the number of rotor blades; c denotes the blade segment chord length; κ denotes the rotor tip loss coefficient; e denotes the flapping hinge offset; Ω denotes the main rotor speed; R denotes the rotor radius; r' denotes the radial length from the blade profile to the flapping hinge; δdenotes the drag coefficient of the blade airfoil; $m_b$denotes the mass of the blade; M_β denotes the mass moment of blade flapping; K_β denotes the equivalent flapping torsion spring stiffness; β denotes the blade flapping angle;I_{MR}denotes the moment of inertia of the rotor; $\overline{U}_T, \overline{U}_P$denote the blade profile normalized tangential and normal airflow velocities, respectively; θ_G denotes the blade profile pitch angle; φ' denotes the blade azimuth angle; *u, v, w* denote the velocities under the body axis system; *p, q* denote the roll and pitch angular velocities under the body axis system, respectively; *g* denotes the acceleration of gravity.

This paper only considers the pitch and flap motion of the rotor blades. The rotor flap motion is simplified to a first-order harmonic quantity. According to the moment balance acting on the flapping hinge, the following blade flapping motion equation can be derived.

$$\begin{aligned} &I_\beta\ddot{\beta} + K_\beta\beta + \left(I_\beta\cos\beta + eM_\beta\right)\Omega^2\sin\beta = \\ &\quad \kappa\int_0^{R-e} \frac{1}{2}\rho ac(\Omega R)^2\left(\overline{U}_T^2\theta_G + \overline{U}_T\overline{U}_P\right)r'dr' \\ &\quad +2\left(I_\beta + eM_\beta\right)\left(p_{HW}\Omega\cos\varphi' - q_{HW}\Omega\sin\varphi'\right) + \\ &I_\beta\left(\dot{p}_{HW}\sin\varphi' + \dot{q}_{HW}\cos\varphi'\right) + M_\beta(\dot{w} - uq + pv - g) \end{aligned} \tag{5}$$

Where I_β denotes the inertia moment of blade flapping; p_{HW}, q_{HW} denote the hub roll and pitch angular velocities under the rotor wind axis system, respectively. By equating the constant term and the coefficient of the first harmonic term on the left and right sides of the equation respectively, the dynamics equation of the rotor disk under the wind shaft system can be derived as,

$$\begin{bmatrix} \ddot{a}_0 \\ \ddot{a}_1 \\ \ddot{b}_1 \end{bmatrix} + \mathbf{D}\begin{bmatrix} \dot{a}_0 \\ \dot{a}_1 \\ \dot{b}_1 \end{bmatrix} + \mathbf{K}\begin{bmatrix} a_0 \\ a_1 \\ b_1 \end{bmatrix} = \mathbf{f} \tag{6}$$

where ***D*** denotes the damping matrix; ***K*** denotes the stiffness matrix; ***f*** denotes the extrinsic motivator vector; a_0, a_1, and b_1 denote the taper, rear, and side angles of the rotor disk, respectively (see details in Ref. [24]).

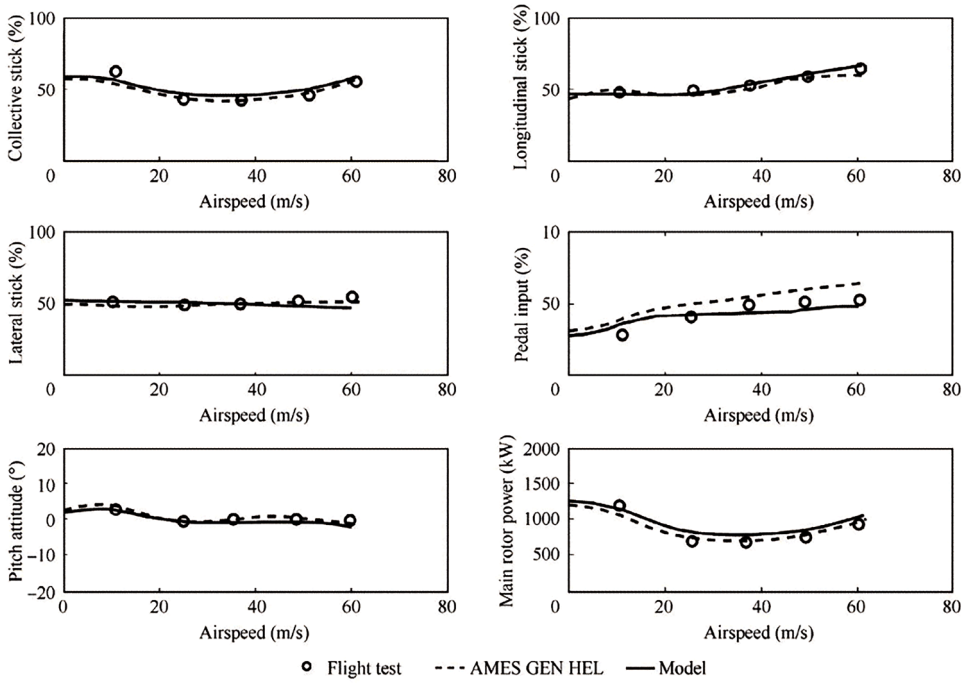

Fig. 2. Model trim validation with flight data and AMES GEN HEL model [23].

1. The aerodynamic force and moment coefficients of the fuselage, horizontal tail, and vertical tail are obtained through interpolation of wind tunnel test data.
2. During the landing phase, the helicopter is affected by ground effect, which requires correction of the rotor-induced velocity using the ground effect factor f_G, expressed as follows [11,25].

$$f_G = 1 - \frac{\sigma a \lambda}{4C_T} \frac{(R/4z)^2}{1 + (\mu/\lambda)^2} \tag{7}$$

In this expression, σ represents rotor solidity; C_T represents rotor thrust coefficient; λ represents the inflow ratio of the rotor; z is the height of rotor hub above the ground; and μ represents the advance ratio of the rotor.

1. In addition, the helicopter may encounter vortex ring state during high-speed descent in landing procedure, which will cause unsteady aerodynamic behavior of rotor. To prevent entering the vortex ring state, it is necessary to keep the main rotor and tail rotor outside the vortex ring region, which can be expressed as a constraint condition [11].

$$\begin{cases} \dfrac{\mu^2 + \lambda^2 - \lambda\nu_0}{\sqrt{\mu^2 + \lambda^2}} \geq -0.28\sqrt{\dfrac{C_T}{2}} \\ \dfrac{\mu_{TR}^2 + \lambda_{TR}^2 - \lambda_{TR}\nu_{0T}}{\sqrt{\mu_{TR}^2 + \lambda_{TR}^2}} \geq -0.28\sqrt{\dfrac{C_{TR}}{2}} \end{cases} \tag{8}$$

Here, μ_{TR} represents the advance ratio of the tail rotor; λ_{TR} is the inflow ratio of the tail rotor; ν_0 and ν_{0T} respectively denote the average non-dimensional induced velocity of the main rotor and tail rotor; C_{TR} is the lift coefficient of the tail rotor.

1. During the safe landing procedure after low tail rotor pitch lockup, the pilot can choose to perform an autorotation landing in the final stage. In this case, the engine throttle is closed to idle mode, and the engine output power P_A and the rotor speed Ω can be described by the following differential equations [11,22],

$$\begin{cases} \dot{P}_A = (0 - P_A)/t_p \\ \dot{\Omega} = \dfrac{P_A - (P_{MR} + P_{TR})/\eta}{(I_{MR} + k^2 I_{TR})\boldsymbol{\Omega}} \end{cases} \tag{9}$$

where t_p represents the engine response time; P_{MR} and P_{TR} denote the required power of the main rotor and tail rotor, respectively; η represents the transmission efficiency; I_{MR} and I_{TR} represent the rotational inertias of the main rotor and tail rotor, respectively; k is the proportionality factor between the main rotor speed and tail rotor speed.

The governing equation of the flight dynamics model is summarized below,

$$\dot{\mathbf{x}}_b = f(\mathbf{x}_b, \mathbf{u}_b, t) \tag{10}$$

where $\mathbf{u}_b = [\delta_{col}; \delta_{lat}; \delta_{lon}; \delta_{ped}]$ is the pilot control vector, δ_{col} denotes collective stick input, δ_{lat} denotes lateral stick input, δ_{lon} denotes longitudinal stick input, and δ_{ped} denotes pedal input, t is time. $\mathbf{x}_b = [\mathbf{x}_F; \mathbf{x}_R; \mathbf{x}_I]$ is the state vector that contains fuselage motion state$\mathbf{x}_F$, rotor flapping state$\mathbf{x}_R$, and rotor inflow state$\mathbf{x}_I$.

$$\begin{cases} \mathbf{x}_F = [u, v, w, p, q, r, \phi, \theta, \psi, x, y, h]^T \\ \mathbf{x}_R = [\dot{a}_0, \dot{a}_1, \dot{b}_1, a_0, a_1, b_1]^T \\ \mathbf{x}_I = [\nu_0, \nu_{1s}, \nu_{1c}]^T \end{cases} \tag{11}$$

Where u, v, w represent the linear velocities of the aircraft body axis system; p, q, r correspond to the angular velocities of the body axis system; ϕ, θ, ψ represent the roll, pitch, and yaw angles, respectively; x, y, h denote the position of the aircraft in the Earth's axis system; and $\nu_0, \nu_{1c}, \nu_{1s}$ represent the non-dimensional terms for rotor uniform inflow, first-order cosine inflow, and first-order sine inflow, respectively.

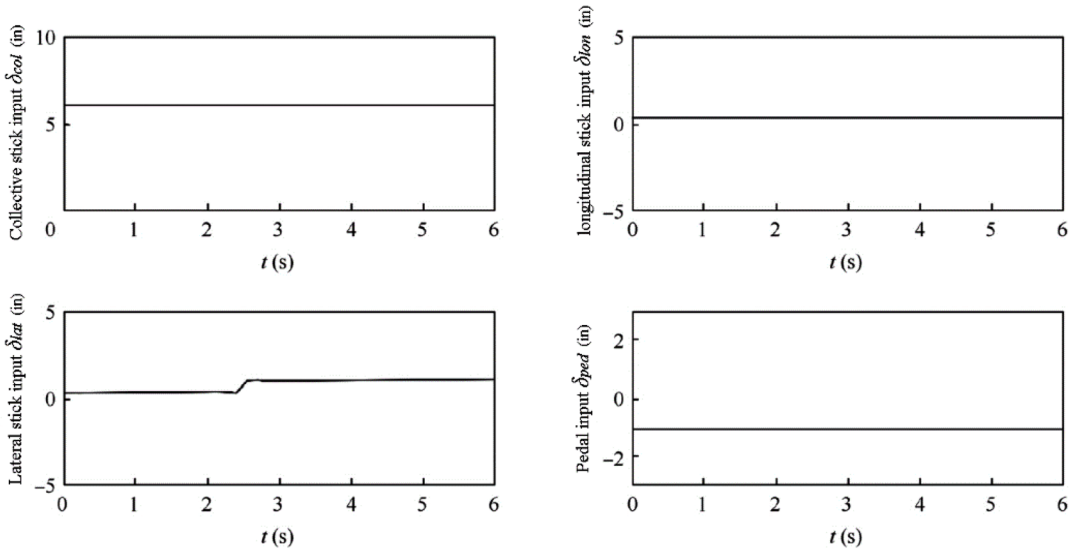

(a) Control inputs

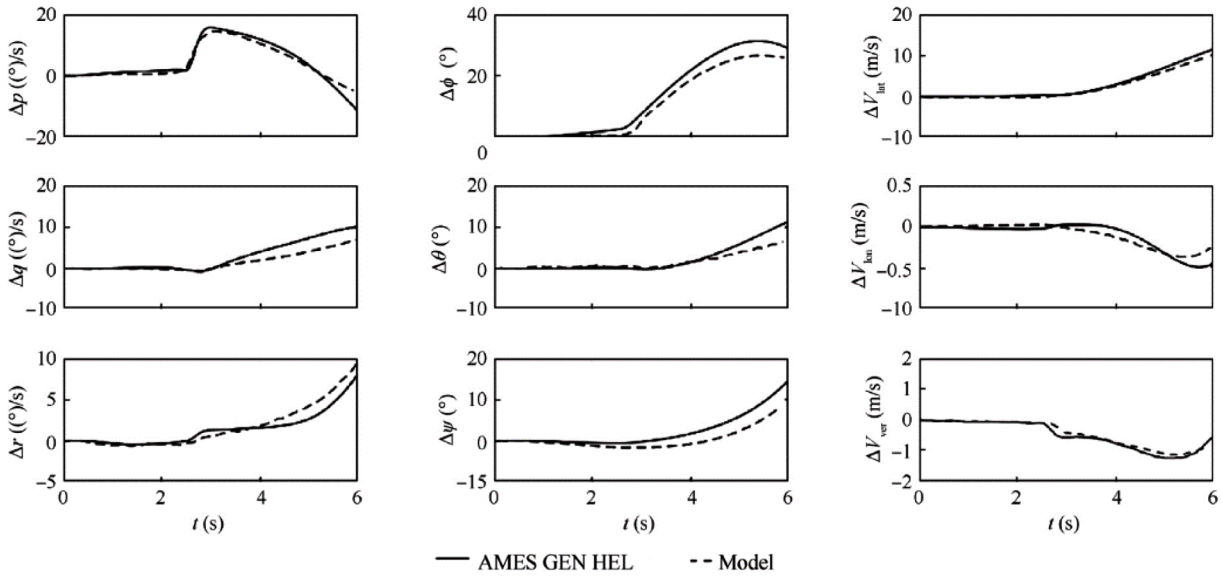

(b) Comparison of transient responses to control inputs

Fig. 3. Model dynamic response validation with AMES GEN HEL model.

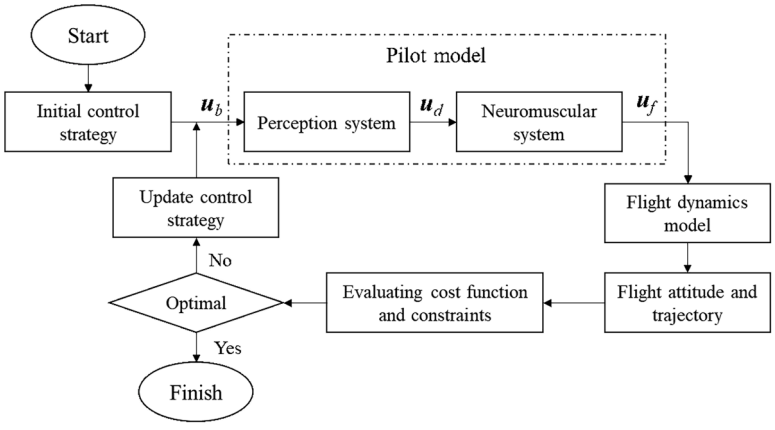

Fig. 4. Schematic diagram of the optimal control model.

2.2. Model validation

Flight test data and the AMES GEN HEL model of the UH-60A helicopter in Ref. [23] are used to validate the steady-state flight dynamics model at an altitude of 1600 m and gross weight of 7257 kg. The trim validation data is obtained from Fig. B1 (UH-60A Black Hawk level-flight static trim) in Ref. [23]. Fig. 2 compares the predicted results to the flight test data and the AMES GEN HEL model. The calculated steady-state variables show good agreement with both the flight test data and the AMES GEN HEL model.

To verify the dynamic response accuracy of the proposed model, transient responses of the UH-60A helicopter AMES GEN HEL simulation in Ref. [23] are used for comparison. The dynamic response data is obtained from Fig. D1 (Comparison of Ames real-time simulation and flight-test data, l-in. right cyclic input at hover). The flight conditions, including weight, center of gravity, inertial moments, and atmospheric environment, are derived from Appendix C. The dynamic response calculated in this study has the same time duration as that reported in Ref. [23]. Fig. 3(a) shows the control inputs, while Fig. 3(b) compares the calculated transient responses of translational velocities, angular velocities, and attitudes with those of the AMES GEN HEL simulation. The results demonstrate that the proposed model can capture the dynamic characteristics of the UH-60A helicopter and has sufficient accuracy in dynamic responses.

3. Nonlinear optimal control method

The nonlinear optimal control model for helicopter landing during tail rotor pitch lockup includes the differential equations constructed from the flight dynamics model and the pilot model, as well as the cost function, path constraints, and boundary conditions formulated based on the flight missions and flight safety requirements.

3.1. Pilot model

To capture the pilot's control strategy for helicopter landing during tail rotor pitch lockup, a corresponding pilot model is developed and integrated into the optimal control model.

The pilot's primary role is to assess the current flight situation and determine suitable control strategies based on the flight mission to maneuver the aircraft. Therefore, a pilot model generally needs to encompass three aspects of the pilot: perception system, control behavior, and neuromuscular system. Given that the optimal control model in this paper can define the desired flight mission via cost function, path constraints, and boundary conditions, and derive appropriate control strategies through numerical solutions, it is assumed that the pilot's control behavior is already encompassed in the optimal control model presented in this paper [26], as illustrated in Fig. 4, where $\boldsymbol{u}_d$ represents the delayed command inputs, and $\boldsymbol{u}_f$ represents the final control input to activate the flight dynamics model. This section solely requires establishing a model that delineates the pilot's perception system and neuromuscular system.

The perception system and neuromuscular system can be represented using the following transfer function:

$$H_p(s) = \frac{1 + T_L s}{1 + T_I s} \cdot \frac{e^{-\tau_p s}}{1 + T_N s} \tag{12}$$

Where T_L represents the feedforward time constant, which reflects the pilot's ability for anticipatory prediction, typically ranges between 0.1 s and 0.6 s, and is set to 0.25 s in this study based on relevant literature [26]. The inertia time constant (T_I) is used to represent the lag effect of the pilot's input displacement on the control stick, generally ranges between 0.2 s and 0.4 s and is also set to 0.25 s in this research. The inertia time constant (T_N) represents the lag caused by the pilot's neuromuscular response, typically ranges between 0.01 s and 0.2 s, and is set to 0.1 s in this study. The delay element ($e^{-\tau_p s}$) reflects the delayed response of the pilot. The delay time (τ_p) is set based on the pilot's capabilities, usually ranges between 0.1 s and 0.25 s, and is set to 0.15 s in this study. Within the pilot's frequency range (0.1–10 rad/s) [24,26], the pure delay element can be approximated using a second-order Pade transfer function.

$$e^{-\tau_p s} \approx \frac{1 - \frac{1}{2}(\tau_p s) + \frac{1}{8}(\tau_p s)^2}{1 + \frac{1}{2}(\tau_p s) + \frac{1}{8}(\tau_p s)^2} \tag{13}$$

In each control input channel, the pilot model can be represented in the following state-space form:

$$\begin{cases} \dot{\mathbf{x}}_p = \mathbf{A}\mathbf{x}_p + \mathbf{B}\mathbf{u}_b \\ \mathbf{u}_f = \mathbf{C}\mathbf{x}_p + \mathbf{D}\mathbf{u}_b \end{cases} \tag{14}$$

Where $\boldsymbol{x}_p$ represents the relevant state variables of the neuromuscular system. The elements of matrices ***A, B, C***, and ***D*** depend on the delay and filter parameters. The above equation can be integrated into the flight dynamics model to reflect the pilot's control actions during landing trajectory and control optimization.

Tail rotor pitch lockup is generally caused by two types of malfunctions: tail rotor control linkage mechanism failure and pedal jamming. The tail rotor control linkage failure cuts off the connection between the pedal and the tail rotor pitch, rendering the pedal ineffective. The pedal jamming, typically caused by tail rotor control mechanism jamming or tail rotor hydraulic booster failure, prevents the pedal from moving and thus makes the pilot unable to control the tail rotor pitch. It can be seen that when the helicopter encounters tail rotor pitch lockup, regardless of the type of malfunction, the tail rotor pitch will be fixed at the current value, and the pedal will be unable to function, the pilot can only control the main rotor collective pitch, lateral cyclic pitch and longitudinal cyclic pitch to perform a safe landing. In this paper, the first-order derivative of the control inputs with respect to time are used as the control variables. In the meantime, the original control inputs are treated as part of the state variables to avoid discontinuities during numerical optimization.

$$\begin{cases} \dot{\delta}_{col} = u_{col} \\ \dot{\delta}_{lat} = u_{lat} \\ \dot{\delta}_{lon} = u_{lon} \end{cases} \tag{15}$$

The basic governing equation of the flight dynamics model (10), Eqs. (14) to (15) form an augmented flight dynamics model for helicopter landing trajectory and control optimization during tail rotor pitch lockup. The differential equation form of the model is as follow,

$$\dot{\mathbf{x}} = f(\mathbf{x}, \mathbf{u}, t) \tag{16}$$

$$\begin{cases} \mathbf{x} = \left[\mathbf{x}_{\mathrm{F}}, \mathbf{x}_{\mathrm{R}}, \mathbf{x}_{\mathrm{I}}, \mathbf{x}_p, \delta_{col}, \delta_{lat}, \delta_{lon}\right]^{\mathrm{T}} \\ \mathbf{u} = \left[u_{col}, u_{lat}, u_{lon}\right]^{\mathrm{T}} \end{cases} \tag{17}$$

3.2. Formulation of optimal control problem

The underactuated optimal control problem for a safe landing during tail rotor pitch lockup can be described as follows: Given the occurrence of tail rotor pitch lockup, the objective is to find a control strategy that satisfies controllability and safety requirements. This strategy should successfully guide the helicopter from its initial state to a specified target state while optimizing a performance index. The corresponding nonlinear optimal control problem (NOCP) can be expressed as follows:

(1) *Optimal variables*: Differential state vector $\boldsymbol{x}$, the control vector $\boldsymbol{u}$, and the free final time t_f (with the initial time t_0 set to 0).
(2) *Cost function*: The cost function of the NOCP serves as the performance index for the entire landing procedure. It is designed to capture the safety and feasibility aspects during the flight and touchdown process, including factors such as variations in flight states, time of flight, and pilot control activity. Since the tail rotor

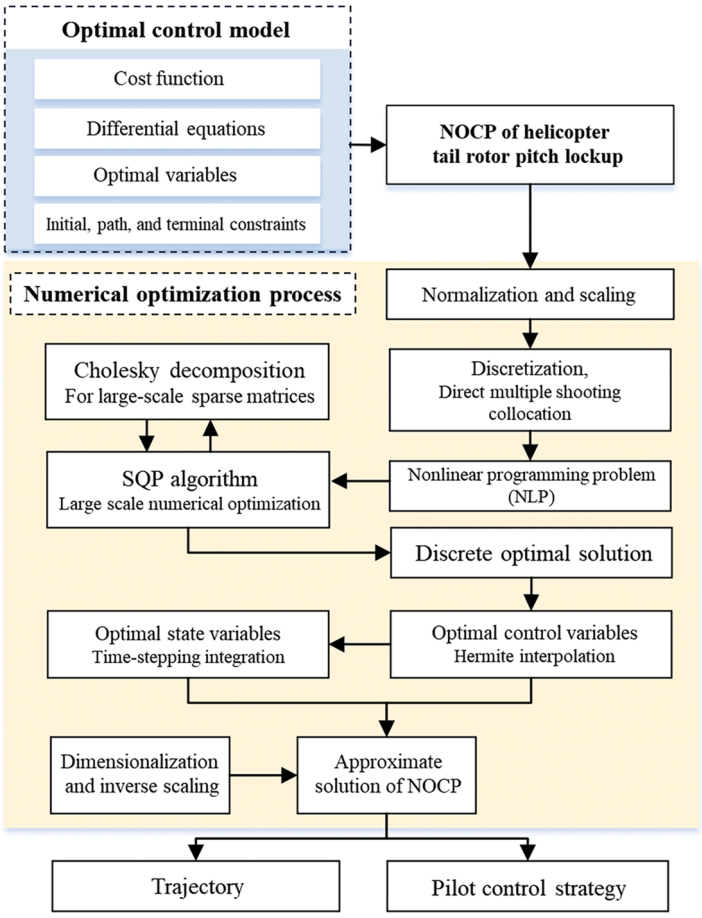

Fig. 5. Numerical optimization process chart.

cannot be manipulated during the lockup condition, the performance index can be defined as below.

$$\begin{aligned}\min J = {} & w_t t_f + w_v\left(u_{e,f}^2 + v_{e,f}^2 + w_{e,f}^2\right) \\ & + \frac{1}{t_f - t_0}\int_{t_0}^{t_f} L(\mathbf{u}(t), \varphi(t), \theta(t), \psi(t))\mathrm{d}t \end{aligned} \tag{18}$$

$$\begin{aligned} & L(\mathbf{u}(t), \varphi(t), \theta(t), \psi(t)) = \\ & w_u \cdot \left(u_{col}^2 \Big/ u_{col,\max}^2 + u_{lon}^2 \Big/ u_{lon,\max}^2 + u_{lat}^2 \Big/ u_{lat,\max}^2\right) + \\ & w_a \cdot \left(\phi^2 \Big/ \phi_{\max}^2 + \theta^2 \Big/ \theta_{\max}^2 + \psi^2 \Big/ \psi_{\max}^2\right) \end{aligned} \tag{19}$$

Where the first and second terms of (18) represent the terminal state performance index, and the third term represents the state and control performance index of the whole optimal landing procedure. $u_{e,f}$, $v_{e,f}$, $w_{e,f}$ are the forward speed, lateral speed, and descent rate of the helicopter at t_f; $u_{col,\max}$,$u_{lon,\max}$,$u_{lat,\max}$are the maximum values of the control variables; $\phi_{\max}$,$\theta_{\max}$,$\psi_{\max}$ are the maximum allowable roll, pitch, and yaw attitude angles respectively; w_t, w_v, w_u and w_a are weighting factors of each item in the performance index. The higher the weight factor, the greater the corresponding term. Therefore, the selection of weight factors needs to be fine-tuned to balance the effects of each term. Since the pilot mainly focuses on controlling the remaining three control variables while also considering changes in the helicopter's attitude angles, w_u and w_a can be relatively larger. Meanwhile, the landing speed limitation can be reflected in the constraint equations, and the flight time can be appropriately extended, so w_t and w_v can be relatively smaller. Based on these considerations, the ranges of the above weight factors can be estimated as:

$$\begin{cases} w_t + w_v + w_u + w_a = 1 \\ 0 \le w_t, w_v \le 1/4 \\ 1/4 \le w_u, w_a \le 1 \end{cases} \tag{20}$$

In this study, we set the time weight (w_t) and terminal velocity weight (w_v) to 0.125, as suggested by Ref. [22]. These weights reflect the urgency of the landing procedure and the need to minimize the landing speed. Subsequently, since the primary objective of this paper is to provide feasible pilot control strategies and serve as a reference for pilots before conducting actual flight tests, we assign a larger weight factor for pilot control activity (w_u) compared to the weight factor for aircraft response (w_a), i.e., $w_u = 0.45$ and $w_a = 0.3$. The simulation results presented in this paper in Sections 4 and 5 demonstrate that the optimal landing trajectory and control process align with the recommendations from actual helicopter flight tests, indicating that the chosen weight factors are reasonably appropriate.

(1) *Constraints*: The constraint equations consist of differential equations, initial boundary conditions, path constraints and terminal constraints.

The differential equations refer to the flight dynamics model (16).

$$\dot{\mathbf{x}} = \mathbf{f}(\mathbf{x}(t), \mathbf{u}(t), t) \quad t \in [t_0, t_f] \tag{21}$$

The initial boundary conditions are determined in the moment of initial pilot control actuation after tail rotor pitch lockup. This paper assumes that the helicopter is in a stable state when encountering tail rotor pitch lockup, and it takes a certain delay time (generally 1 s, Refs.

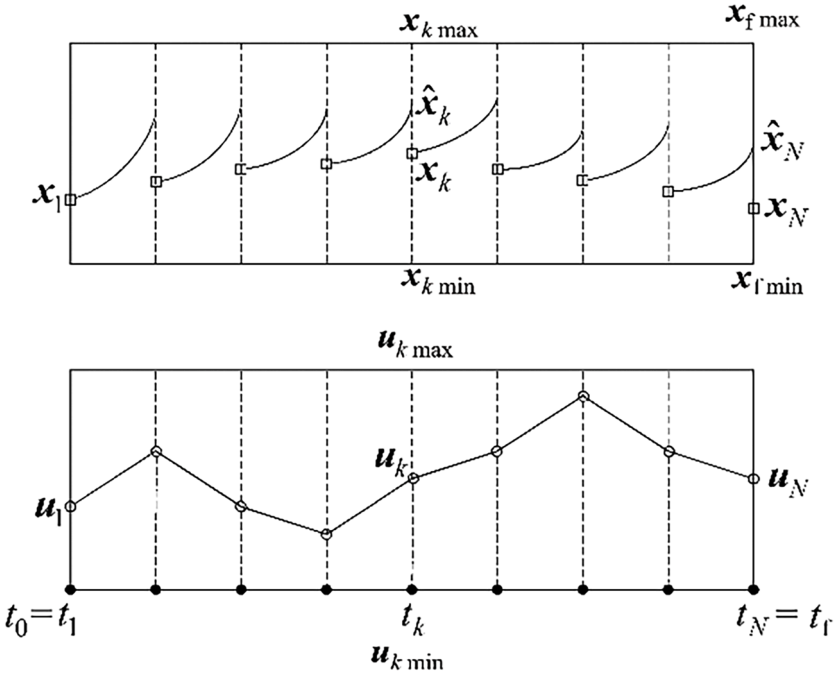

Fig. 6. Direct multiple shooting approach.

[22,27]) for the pilot to start landing operation after discovering the tail rotor control failure. Therefore, the pilot response delay time t_d is considered, and the initial boundary conditions at time t_0 are the variables in the moment after t_d delay.

$$\mathbf{x}(t_0) = \mathbf{x}_{\text{delay}},\ \mathbf{u}(t_0) = \mathbf{u}_{\text{delay}} \tag{22}$$

In fact, tail rotor pitch lockup refers to the mechanism being stuck at the current value, resulting in a frozen control state. In the ideal flight condition assumed in this study, during the pilot delay period, the helicopter still maintains a stable flight state. Therefore, altering the pilot delay time does not influence the subsequent simulation results for the landing trajectory and control optimization.

The terminal constraints are determined by referring to the requirements for safe landing in the helicopter airworthiness regulations [27].

$$\mathbf{x}_{f\min} \le \mathbf{x}(t_f) \le \mathbf{x}_{f\max} \tag{23}$$

Where $\mathbf{x}_{f\min}$, $\mathbf{x}_{f\max}$ are the minimum and maximum values of the state variables at the final time, respectively. The specific values will be given in the case study.

The path constraints can be represented as:

$$\begin{cases} \mathbf{x}_{\min} \le \mathbf{x}(t) \le \mathbf{x}_{\max} \\ \mathbf{u}_{\min} \le \mathbf{u}(t) \le \mathbf{u}_{\max} \end{cases},\quad t \in [t_0, t_f] \tag{24}$$

$$\begin{cases} 0 \le \dfrac{\mu^2 + \lambda^2 - \lambda\nu_0}{\sqrt{\mu^2 + \lambda^2}} + 0.28\sqrt{\dfrac{C_{\text{T}}}{2}} \\ 0 \le \dfrac{\mu_{\text{TR}}^2 + \lambda_{\text{TR}}^2 - \lambda_{\text{TR}}\nu_{0\text{T}}}{\sqrt{\mu_{\text{TR}}^2 + \lambda_{\text{TR}}^2}} + 0.28\sqrt{\dfrac{C_{\text{TR}}}{2}} \end{cases} \tag{25}$$

The path constraints of states are properly selected according to the vortex boundary (8) and specific requirements for rotorcraft of FAR [27]. The constraints of the pilot control rates are selected according to the maximum physical rate limits of the servo booster. The specific values will also be given in the case study.

In the field of engineering applications, NOCPs rarely have analytical solutions and numerical computation methods are usually required to solve them. Numerical methods for NOCP are generally classified into two categories: indirect methods and direct methods. Indirect methods require the derivation of the first-order optimality conditions for the NOCP. However, due to the highly nonlinear and complex nature of the flight dynamics model established in this paper, it is very difficult to obtain the first-order optimality conditions. Direct methods do not require the derivation of the first-order optimality conditions for the NOCP. Instead, they directly approximate the NOCP and transform it into a nonlinear programming problem (NLP) for numerical computation. According to the different discretization methods, direct methods include shooting methods, collocation methods, and differential inclusion methods. Among them, the direct multiple shooting method is suitable for unstable dynamic systems (such as rotorcraft) with a large number of degrees of freedom and high complexity. Therefore, in this paper, the direct multiple shooting method is used to discretize the NOCP into an NLP and solve it numerically.

3.3. Numerical solution techniques

Due to the highly nonlinear and complex nature of the flight dynamics model established in this paper, the nonlinear optimal control model for helicopter landing during tail rotor pitch lockup involves numerous state and control variables, as well as intricate constraint equations and cost function. This necessitates the design of a high-convergence numerical optimization method for solving the problem.

As depicted in Fig. 5, this study employs the direct multiple shooting collocation method to generate discretization nodes and utilizes the Sequential Quadratic Programming (SQP) algorithm for numerical solution. To handle large-scale sparse matrices, Cholesky decomposition is used to reduce computational complexity and data storage requirements. The outcome of this approach is an approximation of the pilot control strategy and flight trajectory for the optimal control problem. The specific numerical optimization process can be described as follows:

Firstly, in order to improve the convergence of numerical optimization, normalization and scaling of the optimal variables in NOCP are applied as follows,

Table 2
Path constraints in landing.

Constraints	Min	Max	Constraints	Min	Max
$u(t)$(m/s)	0	40	$h(t)$(m)	0	20
$v(t), w(t)$(m/s)	−20	20	$y(t)$(m)	−10	10
$p(t), q(t), r(t)$(°/s)	−20	20	$x(t)$(m)	0	200
$\varphi(t), \theta(t), \psi(t)$(°)	−20	20	$\delta_{col,lon,lat,ped}(t)$(%)	0	100
$\overline{\Omega}(t)$	0.8	1.1	$u_{col,lon,lat,ped}(t)$(%/s)	0	25

Table 3
Terminal constraints in landing.

Constraints	Min	Max	Constraints	Min	Max
$p(t_f), q(t_f), r(t_f)$(°/s)	−5	5	$\theta(t_f)$(°)	−5	10
$\varphi(t_f), \psi(t_f)$	−2	2	$\dot{y}(t_f)$(m/s)	−1	1
$\dot{x}(t_f)$(m/s)	0	12.2	$\dot{h}(t_f)$(m/s)	−1.5	0
$h(t_f)$(m)	0	0			

$$\begin{cases} (\overline{u},\overline{v},\overline{w}) = \dfrac{1}{k_v\Omega_0 R}(u,v,w),\ (\overline{p},\overline{q},\overline{r}) = \dfrac{k_x}{k_v\Omega_0}(p,q,r) \\ (\dot{\overline{a}}_0,\dot{\overline{a}}_1,\dot{\overline{b}}_1) = \dfrac{k_x}{k_v\Omega_0}(\dot{a}_0,\dot{a}_1,\dot{b}_1),\ (\overline{x},\overline{y},\overline{h}) = \dfrac{1}{k_x R}(x,y,h), \\ \overline{\Omega} = \dfrac{\Omega}{\Omega_0},\ \overline{P}_A = \dfrac{k_x}{k_v\Omega_0^3\left(I_{MR}+k^2 I_{TR}\right)}P_A,\ \tau = \dfrac{k_v\Omega_0}{k_x}t \\ \overline{\mathbf{u}} = \dfrac{k_x}{k_v\Omega_0}\mathbf{u} \end{cases} \tag{26}$$

where Ω_0 is the helicopter standard rotor speed. To make the normalized-scaled optimal variables close to one in value, take k_x=10 and k_v=0.1, The specific non-dimensional scaling process can be found in Ref. [11].

The direct multiple shooting collocation method [28] is applied by breaking the continuous landing procedure into discrete time nodes and segments. The discretizing process is shown in Fig. 6.

According to Fig.6, the solution time interval $[t_0, t_f]$ is discretized into N equally spaced nodes, the corresponding NLP variables are

$$\mathbf{X} = \left[(\mathbf{x},\mathbf{u})_1, (\mathbf{x},\mathbf{u})_2, ..., (\mathbf{x},\mathbf{u})_k, ..., (\mathbf{x},\mathbf{u})_N, t_f\right] \tag{27}$$

At the k-th time interval, the differential equations of the flight dynamics model (21) are integrated in a time-stepping manner (from t_k to t_{k+1}), and "shooting" is performed with the discretized design variables at the nodes. This integration has the advantage of decreasing the cost for computing finite differencing by increasing the problem sparsity [28], which helps to stabilize the integration of the unstable systems, especially for rotorcraft vehicles. The shooting of discrete time segment k (denoted by$\mathbf{x}_{k+1}$) can be described as,

$$\mathbf{x}_{k+1} - \widehat{\mathbf{x}}_{k+1} = \mathbf{0},\ k = 1, \cdots, N-1 \tag{28}$$

$$\widehat{\mathbf{x}}_{k+1} = \mathbf{x}_k + \int_{t_k}^{t_{k+1}} f(\mathbf{x},\mathbf{u},t)dt \tag{29}$$

During the integration process, the control variable $\mathbf{u}(t)$ is obtained through linear interpolation with $\mathbf{u}_k$ and $\mathbf{u}_{k+1}$. This method not only guarantees that the discretized model is as close as possible to the original nonlinear model, but also helps to increase the sparsity of the NLP and reduce the computational cost of finite difference methods.

The cost function of NOCP is also discretized as the sum of piecewise integrations:

$$\min J = w_t t_N + w_v\left(u_{d,N}^2 + v_{d,N}^2 + w_{d,N}^2\right) + \frac{1}{t_f - t_0}\sum_{k=1}^{N-1}\int_{t_k}^{t_{k+1}} L(\mathbf{u},\varphi,\theta,\psi)\mathrm{d}t \tag{30}$$

The constraints are enforced on the corresponding time nodes of $\boldsymbol{X}_k$.

$$\mathbf{x}_{f\min} \le \mathbf{x}(t_N) \le \mathbf{x}_{f\max} \tag{31}$$

$$\begin{cases} \mathbf{x}_{\min} \le \mathbf{x}(t_k) \le \mathbf{x}_{\max} \\ \mathbf{u}_{\min} \le \mathbf{u}(t_k) \le \mathbf{u}_{\max} \end{cases} \tag{32}$$

$$\begin{cases} 0 \le \dfrac{\mu_k^2 + \lambda_k^2 - \lambda_k\nu_{0,k}}{\sqrt{\mu_k^2+\lambda_k^2}} + 0.28\sqrt{\dfrac{C_{T,k}}{2}} \\ 0 \le \dfrac{\mu_{TR,k}^2 + \lambda_{TR,k}^2 - \lambda_{TR,k}\nu_{0T,k}}{\sqrt{\mu_{TR,k}^2+\lambda_{TR,k}^2}} + 0.28\sqrt{\dfrac{C_{TR,k}}{2}} \end{cases} \tag{33}$$

The nonlinear programming problem can be effectively solved using SQP algorithm [29] to get the approximate solution of the original NOCP. To improve the accuracy of the optimal solution, the optimal state variables $\boldsymbol{x}(t)$ are calculated by integrating the flight dynamics model (21) from t_0 to t_f with piecewise linear interpolation of $(\mathbf{u}_1, \mathbf{u}_2, ..., \mathbf{u}_k, ..., \mathbf{u}_N)$.

3.4. Validation of optimal control method

Currently, there is a lack of research on the landing trajectory and control optimization for piloted helicopters experiencing tail rotor pitch lockup. Therefore, we have utilized flight test data from the UH-60A helicopter's conventional autorotation [22] to validate the effectiveness of flight dynamics model, pilot model and optimal control approach. While there is a clear distinction between safe landing during tail rotor pitch lockup and conventional autorotation, both scenarios involve an autorotation landing procedure after engine shutdown. As a result, the comparison still demonstrates the effectiveness of safe landing during tail rotor pitch lockup to some extent.

The conditions are steady-state with weight of 7239 kg, altitude of 9.1 m, standard atmospheric environment, forward speed of 0 m/s, track angle of 0°, no sideslip and pilot delay time of 1.2 s. The landing procedure lasted about 5 s because the altitude was set low for the safe autorotation landing test.

The specific path constraints are as follows, where all the variables take the SI units (Tables 2, 3)

The terminal constraints are:

The optimal landing procedure is calculated and compared with the flight test data (Ref. [22]) as shown in Fig. 7. It can be found that the optimal landing procedure is close to the flight test data, which indicates that the flight dynamics model, pilot model and optimal control approach applied in this paper are feasible.

4. Landing optimization in high tail rotor pitch lockup

4.1. Case study

This section provides a computational analysis of the optimal landing trajectory and control strategy for a helicopter encountering high tail rotor pitch lockup, which typically occurs during hovering, low-speed flight, and climbing. The UH-60A helicopter in Ref. [23] is used as the sample helicopter with gross weight of 7257 kg. In this case study, we assume that the helicopter is in a stable flight at a low speed of 2 m/s at an altitude of 50 m with a heading angle of 0° in standard atmospheric condition. Then, the tail rotor is suddenly stuck at high pitch, rendering it uncontrollable. After a delay of 1 s, the pilot uses the remaining three controls to safely land the helicopter.

The initial boundary conditions are the state and control variables of the helicopter after experiencing high tail rotor pitch lockup for 1 s delay. Considering the specific requirements for a safe landing [27], the terminal constraints are determined as shown in Table 4.

Considering the flight mission, safety and control system characteristics, the path constraints are proposed in Table 5.

In addition, the constraint Eq. (8) for vortex ring state boundary is

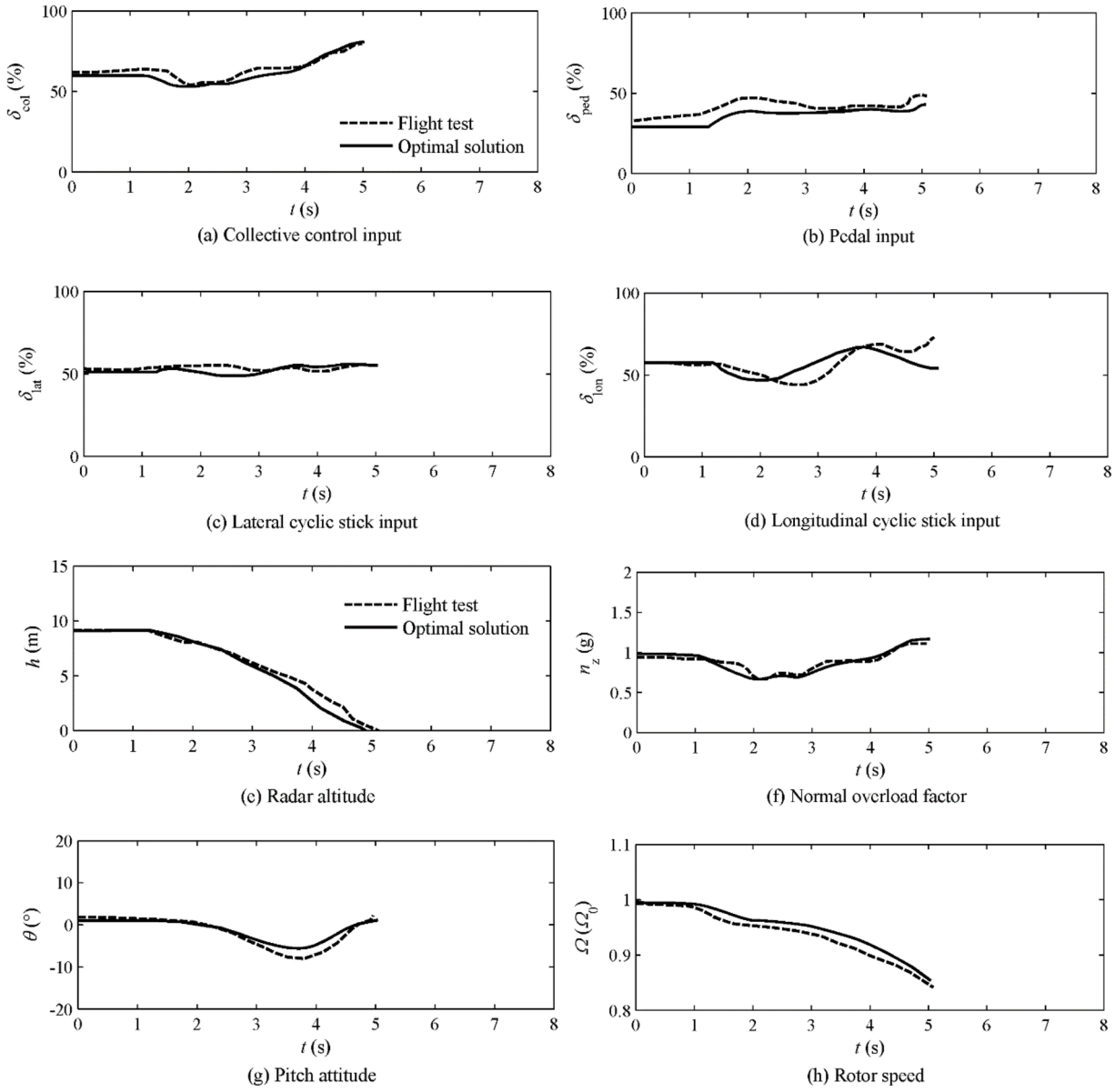

Fig. 7. Comparison of optimal solution and flight test data [22] for autorotation landing in OEI.

Table 4
Terminal constraints in landing.

Constraints	Min	Max	Constraints	Min	Max
$p(t_f)(\circ/\mathrm{s})$	−5	5	$\dot{x}(t_f)(\mathrm{m/s})$	0	12.2
$q(t_f)(\circ/\mathrm{s})$	−5	5	$\dot{y}(t_f)(\mathrm{m/s})$	−1.524	1.524
$r(t_f)(\circ/\mathrm{s})$	−5	5	$\dot{h}(t_f)(\mathrm{m/s})$	−1.524	0
$\phi(t_f)(\circ)$	−5	5	$h(t_f)(\mathrm{m})$	0	0
$\theta(t_f)(\circ)$	−5	10			

Table 5
Path constraints in landing.

Constraints	Min	Max	Constraints	Min	Max
$u(t)(\mathrm{m/s})$	0	20	$h(t)(\mathrm{m})$	0	60
$v(t), w(t)(\mathrm{m/s})$	−10	10	$y(t)(\mathrm{m})$	−50	50
$p(t), q(t), r(t)(\circ/\mathrm{s})$	−20	20	$x(t)(\mathrm{m})$	0	200
$\varphi(t), \theta(t)(\circ)$	−30	30	$\delta_{col,lon,lat,ped}(t)(\%)$	0	100
$\psi(t)(\circ)$	−90	90	$u_{col,lon,lat,ped}(t)(\%/\mathrm{s})$	0	25

Table 6
Weight factors selected.

Weight factor	Description	Value
w_t	Weight factor for flight time	0.125
w_v	Weight factor for touchdown speed	0.125
w_u	Weight factor for pilot control activity	0.45
w_a	Weight factor for attitude changes	0.30

also included to avoid entering the vortex ring state.

Based on the analysis and conclusions in Section 3.2 of this paper, as well as previous simulation debugging, the weight factors for performance index (18) are selected as shown in Table 6.

In the case study of landing optimization in high tail rotor pitch lockup, a sampling time of 0.36 s (sampling frequency of 2.78 Hz, with 30 discrete points) was used. Through extensive simulations, it was observed that when the number of discrete points N exceeded 30, the numerical simulation results remained essentially unchanged, while the computational efficiency rapidly decreased. Additionally, the frequency range commonly used by pilots is between 0.1 and 10 rad/s (0.016–1.6

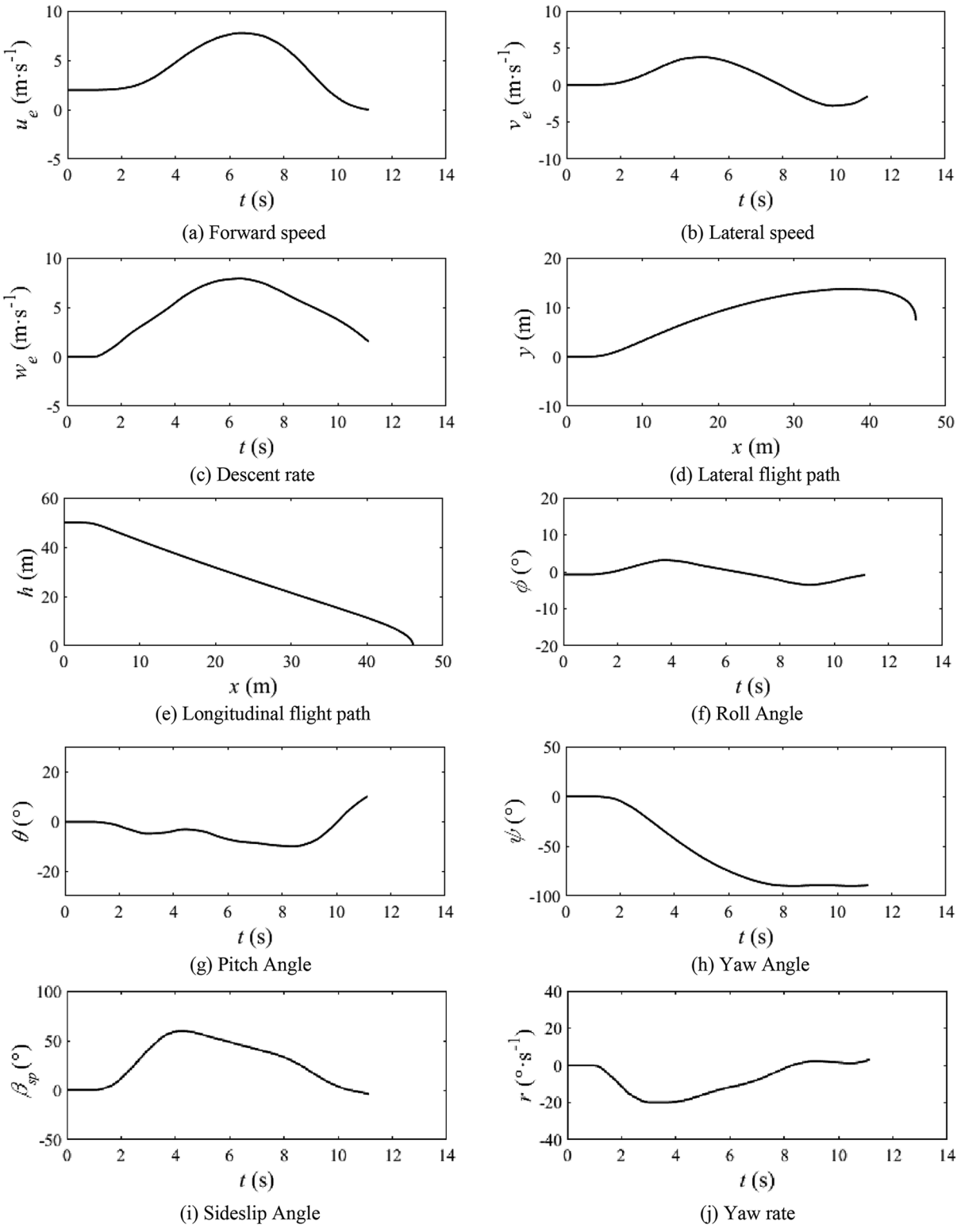

Fig. 8. State variables of optimal landing procedure in high tail rotor pitch lockup.

Hz), which is lower than the sampling frequency in this study. Therefore, the optimization results of pilot control strategies can adequately reflect their manipulation behavior, indicating that the selected sampling time is reasonable.

Figs. 8 and 9 show the optimal landing process of the sample helicopter encountering high tail rotor pitch lockup. Where u_e, v_e, w_e denote the ground-axis forward velocity, lateral velocity, and descent rate, respectively; β_{sp} refers to the helicopter's body slip angle; P_R represents the power required by the helicopter.

The results are concluded in Table 7 from Figs. 8 and 9.

The optimal landing trajectory and control process obtained in this study are generally consistent with the suggestions for safe landing in high tail rotor pitch lockup, as proposed in actual flight tests (Refs. [4,5,10]). That is when the tail rotor is stuck in a large pitch angle, staying in

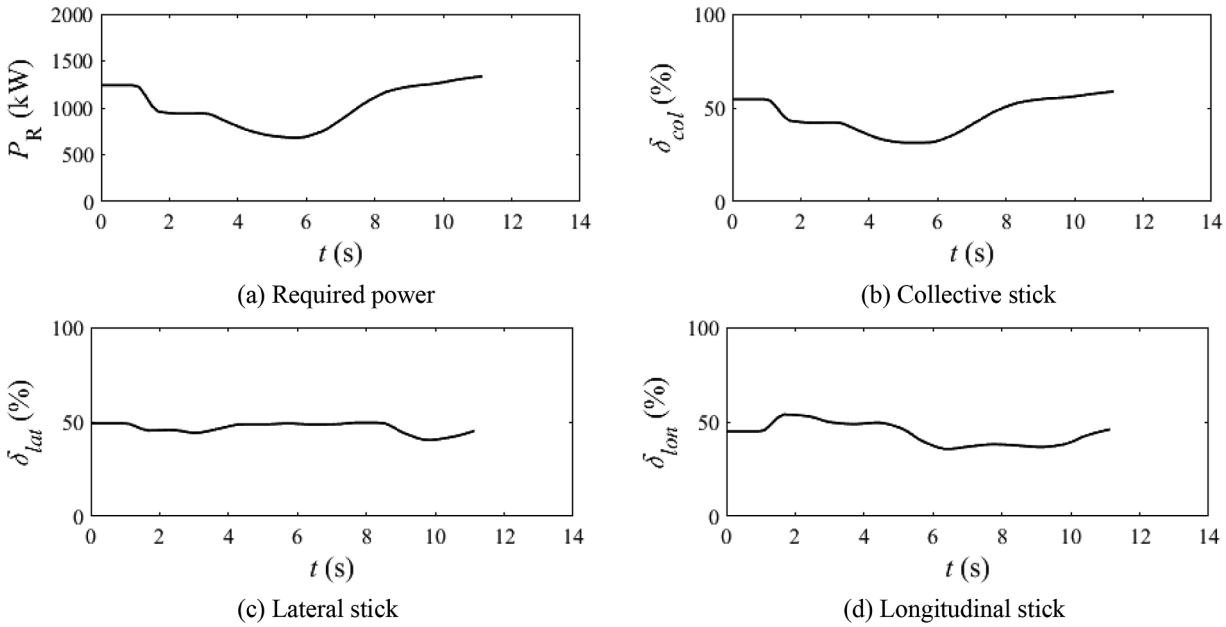

Fig. 9. Required power and controls of optimal landing procedure in high tail rotor pitch lockup.

Table 7
Results drawn from optimal landing procedure in high tail rotor pitch lockup.

Stage	Pilot control	Flight state	Time of duration
Pilot delay period	No control	Stable flight in a frozen state	0 ~ 1 s
Oblique downward flight	1. Reduces the main rotor collective pitch (Fig. 9b), and uses longitudinal cyclic pitch to make the helicopter enter an oblique downward flight (Fig. 8e); 2. Stabilizes the roll angle by making slight adjustments to the lateral cyclic pitch stick (Fig. 9c).	1. The power required decreases (Fig. 9a), the torque of the rotor decreases, and the relatively large lateral force of the tail rotor causes the helicopter to yaw to the left (Fig. 8h–j), resulting in a large-angle sideslip flight; 2. At the same time, the helicopter has a small right roll response during the descent (Fig. 8f), mainly caused by the main rotor lateral flapping.	1–4 s
Preparation for landing	1. Gradually increases the main rotor collective pitch; 2. Then the slightly pulls the longitudinal stick back to slow down and prepares for the final landing touchdown (Fig. 9d).	1. The negative torque of the main rotor increases, so the previously unfavorable yaw rate and negative sideslip angle gradually decrease; 2. The helicopter gradually rolls to the left to balance the tail rotor thrust.	4–8.6 s
Precise landing	Continues to slightly increase the main rotor collective pitch (Fig. 9b) and manipulates the helicopter to stabilize its attitude, preparing to land vertically (Fig. 8a, b).	1. The helicopter lands almost vertically (Fig. 8e), and the descent rate is close to 0 m/s at the moment of touchdown (Fig. 8c).	8.6–11 s

Table 8
Terminal constraints in conventional landing.

Constraints	Min	Max	Constraints	Min	Max
$p(t_f)(\circ/s)$	−15	15	$\dot{x}(t_f)(m/s)$	0	12.2
$q(t_f)(\circ/s)$	−15	15	$\dot{y}(t_f)(m/s)$	−3.048	3.048
$r(t_f)(\circ/s)$	−40	40	$\dot{h}(t_f)(m/s)$	−1.524	0
$\phi(t_f)(\circ)$	−5	5	$h(t_f)(m)$	0	0
$\theta(t_f)(\circ)$	−5	10			

Table 9
Path constraints in conventional landing.

Constraints	Min	Max	Constraints	Min	Max
$u(t)(m/s)$	0	50	$h(t)(m)$	0	60
$v(t), w(t)(m/s)$	−20	20	$y(t)(m)$	−50	50
$p(t), q(t)(\circ/s)$	−20	20	$x(t)(m)$	0	400
$r(t)(\circ/s)$	−60	60	$\delta_{col,lon,lat,ped}(t)(\%)$	0	100
$\varphi(t), \theta(t)(\circ)$	−40	40	$u_{col,lon,lat,ped}(t)(\%/s)$	0	25
$\psi(t)(\circ)$	−90	90			

Table 10
Constraints at a height of 3 m, before autorotation.

Constraints	Min	Max	Constraints	Min	Max
$p(t_h), q(t_{h_1}), r(t_h)(^\circ/s)$	0	0	$\dot{p}(t_h), \dot{q}(t_h), \dot{r}(t_h)(^\circ/s)$	0	0
$\dot{u}(t_h), \dot{v}(t_h), \dot{w}(t_h)(m/s)$	0	0	$h(t_h)(m)$	3	3

a high-power state (low speed) helps to maintain directional stability. The main rotor collective pitch can be manipulated to maintain direction and sideslip angle until touchdown. This indicates that the numerical simulation results in this section are reasonable.

4.2. Discussion

The landing of piloted helicopters during high tail rotor pitch lockup is a critical situation that may result in loss of control and accidents. Therefore, comprehending how to manage it is vital for helicopter safety and performance. These findings offer an in-depth insight into the landing trajectory and control optimization for such helicopters. The

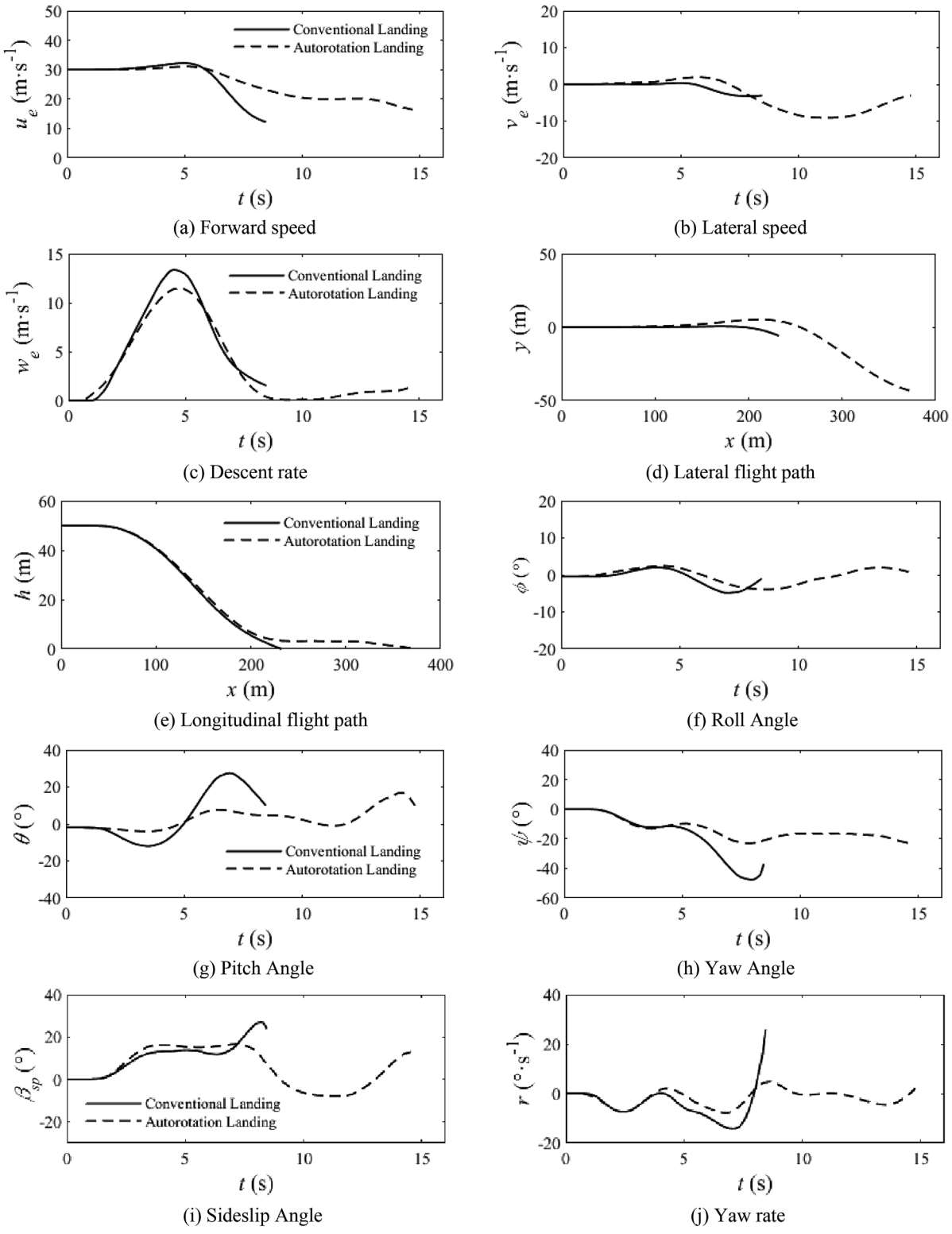

Fig. 10. State variables of optimal landing procedure in low tail rotor pitch lockup.

optimized trajectories and control strategies contribute to the safety and performance of helicopters in several ways:

1. Oblique downward flight: The pilot reduces the main rotor collective pitch and uses longitudinal cyclic pitch to control the helicopter's descent. This allows for a controlled and safe descent, reducing the risk of a crash.
2. Preparation for landing: The pilot gradually increases the main rotor collective pitch to balance the negative torque of the main rotor and the lateral force of the tail rotor. This helps to stabilize the helicopter's yaw and sideslip, maintaining control and direction.
3. Precise Landing: The pilot manipulates the helicopter to land almost vertically, with the descent rate close to 0 m/s at the moment of touchdown. This precise control during the landing phase reduces

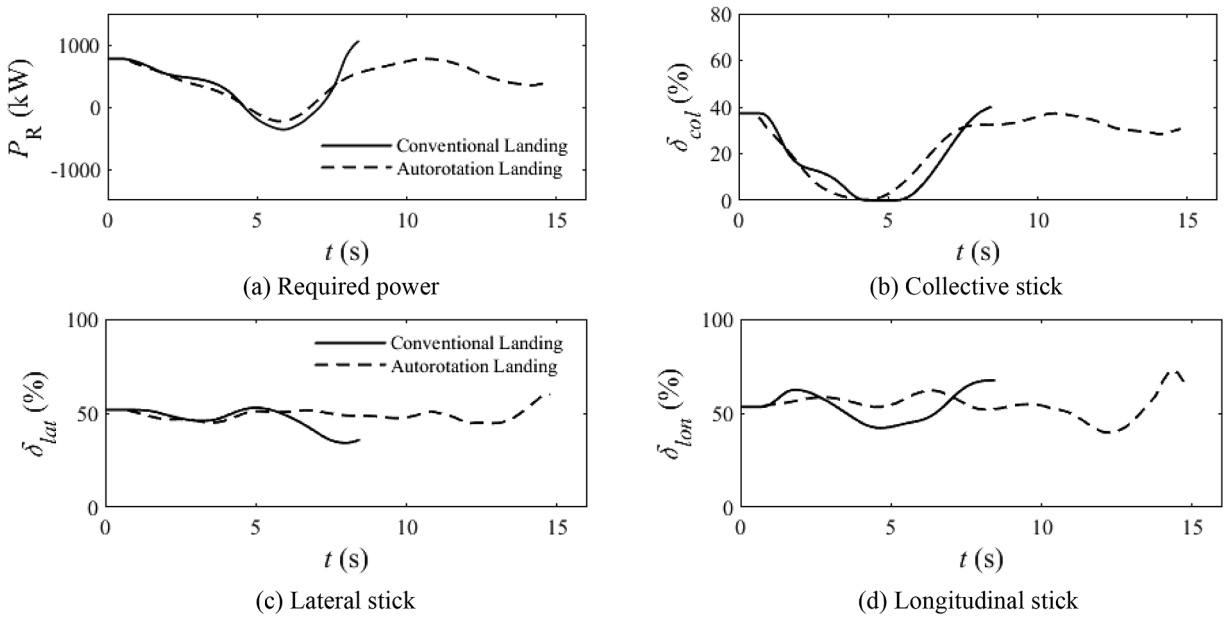

Fig. 11. Required power and controls of optimal landing procedure in low tail rotor pitch lockup.

the risk of damage to the helicopter and ensures the safety of the pilot and any passengers.

4. Validation of flight test suggestions: The optimal landing trajectory and control process obtained in this study align with the suggestions for safe landing in high tail rotor pitch lockup from actual flight tests. This validates the effectiveness of these strategies and provides a practical guide for pilots facing such situations.

In conclusion, these findings provide valuable insights into how to handle high tail rotor pitch lockups, enhancing the safety and performance of helicopters in such situations. They also contribute to the broader understanding of helicopter control and flight dynamics, which can inform future research and development in this field.

5. Landing optimization in low tail rotor pitch lockup

5.1. Case study

This section analyzes the optimal landing trajectory and control process for a helicopter experiencing low tail rotor pitch lockup. Low tail rotor pitch lockup generally corresponds to low power flight states such as descent or economical speed flight. The UH-60A helicopter in Ref. [23] is used as the sample helicopter with gross weight of 7257 kg. In this case study, it is assumed that the helicopter is in a stable flight at a height of 50 m and a track angle of 0° at an economic speed of 30 m/s in standard atmospheric conditions. Then, the tail rotor is suddenly stuck at low pitch and cannot be controlled. The pilot uses the remaining three control inputs to safely land the helicopter after a delay of 1 s.

When a low tail rotor pitch lockup occurs, the pilot can choose a conventional landing or an autorotation landing at a height of 2–3 m from the ground. Therefore, this paper discusses and analyzes these two methods respectively.

(1) Conventional landing

The initial boundary conditions are the state and control variables of the helicopter after experiencing low tail rotor pitch lockup for 1 s delay. During conventional landing, insufficient lateral force from the tail rotor can result in higher body angular velocities (especially yaw rate r) when touching down. Considering the requirements for safe landing, this paper sets the following terminal constraints as shown in Table 8.

Considering the flight mission, safety and control system characteristics, the following path constraints are proposed as shown in Table 9.

In addition, the constraint Eq. (8) for vortex ring state boundary is also included to avoid entering the vortex ring state.

(1) Autorotation landing at 3 m above ground

According to the description in Refs. [4,5,10], when a low tail rotor pitch lockup occurs, the pilot can choose an autorotation landing at a height of 2, 3 m from the ground. Autorotation landing is a complex emergency maneuver. In order to reduce the difficulty of operation, this paper assumes that the helicopter is in a stable flight at a height of 3 m (at time t_h) before performing the autorotation landing, the corresponding constraints are as follows: (Table 10).

Based on the assumption of stable flight at a height of 3 m, the trajectory and control optimization for autorotation landing are further conducted. During autorotation optimization, the engine is set in idle mode, so the corresponding differential equation of engine output shaft power and rotor speed (9) is included. For comparison, the boundary conditions, path constraints, and performance indexes of autorotation landing are consistent with conventional landing.

During autorotation landing, the helicopter can use the rotational kinetic energy stored in the rotor to land safely. However, if the rotor speed is too high, the advancing blades will experience compressibility effect, causing a sudden increase in drag. On the other hand, if the rotor speed is too low, the blades may stall, leading to a significant decrease in rotor lift. Therefore, the limitation of the rotor speed is incorporated into the path constraints, as shown below (Ref. [22]).

$$0.9 \leq \overline{\Omega}(t) \leq 1.1 \tag{34}$$

In the case study of landing optimization in low tail rotor pitch lockup, the conventional landing optimization corresponds to a sampling time of 0.3 s (sampling frequency of 3.3 Hz, with 30 discrete points), while the autorotation landing optimization corresponds to a sampling time of 0.3 s (sampling frequency of 3.3 Hz, with 50 discrete points). Both of these sampling times are higher than the frequency range commonly used by pilots. Hence, these two sampling times are also considered reasonable.

Figs. 10 and 11 show the optimal landing process of the sample helicopter encountering low tail rotor pitch lockup.

The results are concluded in Tables 11 and 12 from Figs. 10 and 11.

Table 11
Results for conventional landing optimization in low tail rotor pitch lockup.

Stage	Pilot control	Flight state	Time of duration
Pilot delay period	No control	Stable flight in a frozen state	0 ~ 1 s
Oblique downward flight	1. Reduces the main rotor collective pitch (Fig. 11b) to decrease the rotor torque, and uses longitudinal stick (Fig. 11d) to make the helicopter enter an oblique downward flight (Fig. 10e); 2. Stabilize the roll angle by making slight adjustments to the lateral cyclic pitch stick (Fig. 11c).	1. The relatively large lateral force of the tail rotor causes the helicopter to yaw to the left (Fig. 10h–j), resulting in a small-angle sideslip flight; 2. At the same time, the helicopter will also have a small right roll response (Fig. 10f).	1–2.5 s
Preparation for landing	1. Reduces the main rotor collective pitch to its minimum setting, then gradually increases it in order to reduce the rate of descent (Fig. 11b); 2. Controls the longitudinal cyclic pitch stick (Fig. 11d) to reduce the forward speed to the maximum allowed value for landing (Fig. 10a) in order to minimize the required power (i.e., main rotor torque) at touchdown.	1. The descent rate begins to decrease, and the lateral velocity has increased slightly (Fig. 10b, c); 2. Before final landing, the larger negative rotor torque still causes the yaw angle and yaw rate to increase (Fig. 10h–j).	2.5–5 s
Precise landing	Pushes the longitudinal stick forward to decrease the pitch angle within the allowable range of landing attitude (Fig. 11d).	1. At this point, the lateral velocity and descent rate are both close to 0 m/s (Fig. 10b, c) at touchdown; 2. However, the larger negative rotor torque at touchdown still causes the yaw rate to increase to nearly −30°/s (Fig. 10j), which can easily cause danger.	5–9 s

Table 12
Results for autorotational landing optimization in low tail rotor pitch lockup.

Stage	Pilot control	Flight state	Time of duration
Pilot delay period	No control	Stable flight in a frozen state	0 ~ 1 s
Oblique downward flight	1. Reduces the main rotor collective pitch (Fig. 11b) to decrease the rotor torque, and uses longitudinal stick (Fig. 11d) to make the helicopter enter an oblique downward flight (Fig. 10e); 2. Stabilize the roll angle by making slight adjustments to the lateral cyclic pitch stick (Fig. 11c); 3. Basically the same as that in the conventional landing process, but with smaller amplitude (Fig. 11c, d).	1. The relatively large lateral force of the tail rotor causes the helicopter to yaw to the left (Fig. 10h–j), resulting in a small-angle sideslip flight; 2. At the same time, the helicopter will also have a small right roll response; 3. Compared to conventional landing, the helicopter's roll and pitch attitudes change more gradually (Fig. 10f, g).	1–3 s
Preparation for autorotational landing	1. Reduces the main rotor collective pitch to its minimum setting, then gradually increases it in order to reduce the rate of descent (Fig. 11b); 2. Manipulates the longitudinal cyclic pitch stick (Fig. 11d) to guide the helicopter into a stable flight.	1. The descent rate begins to decrease, and the lateral velocity has increased slightly; 2. The required power has been maintained at a low level, so the yaw rate is basically maintained at around 0°/s (Fig. 10j); 3. At 10 s, the helicopter is in a stable flight at a height of 3 m and is ready for autorotational landing.	3–10 s
Autorotational landing	1. Switches the engine throttle into idle mode, and pulls the longitudinal stick backwards (Fig. 11d) to further reduce the forward speed of the helicopter (Fig. 10a); 2. Fine-tune the main rotor collective pitch to land slowly (Fig. 11b), while continuing to maintain a stable attitude (Fig. 10 g).	1. 1.The lateral velocity and descent rate are both close to 0 m/s at touchdown (Fig. 10b, c); 2. The yaw rate is also approaching 0°/s (Fig. 10j), making the landing safer. This is because the engine no longer outputs torque to the main rotor, so the helicopter can still maintain a stable yaw attitude during landing.	10–15 s

The optimal landing trajectory and control process obtained in this section are generally consistent with the recommendations for safe landing after low tail rotor pitch lockup in actual helicopter flight tests (Refs. [4,5,10]). That is, when the tail rotor is stuck at a low pitch angle, direction balance can be maintained in a low power state (near economic speed), but it is not conducive to a safe landing afterwards. During the landing process, a larger sideslip and descent rate should be used to approach the landing area, and the horizontal speed should be appropriately increased before touchdown to prioritize ensuring that the vertical speed and landing attitude are within limits at the moment of touchdown, which could be dangerous. Alternatively, when the height drops to about 2–3 m, the throttle should be closed to idle to perform autorotational landing. At this time, the landing will be safer with a much lower yaw rate at touchdown. This case study shows that the numerical simulation results in this section are reasonable.

5.2. Discussion

These findings in Section 5.1 are significant as they offer a comprehensive understanding of landing trajectory and control optimization for piloted helicopters facing low tail rotor pitch lockup. The optimized trajectories and control strategies contribute to the safety and performance of helicopters in several ways:

1. Maintaining stability: The study shows that during both conventional and autorotational landings, the pilot maintains a stable flight by making necessary adjustments to the main rotor collective pitch and cyclic pitch stick. This is important as it gives the pilot control over the helicopter's descent and direction, reducing the risk of a crash.
2. Oblique downward flight: The pilot gradually reduces the main rotor collective pitch to control the helicopter's descent rate and forward speed. This allows for a controlled and safe descent, reducing the risk of damage to the helicopter and ensuring the safety of the pilot and any passengers.
3. Safe landing: The pilot manipulates the helicopter to land with lateral velocity and descent rate close to 0 m/s, which reduces the risk of damage to the helicopter and ensures the safety of the landing.
4. Autorotation advantage: The autorotational landing strategy, which involves the engine no longer outputting torque to the main rotor, allows the helicopter to maintain a stable yaw attitude during landing, resulting in a safer landing with a much lower yaw rate at touchdown.
5. Validation of flight test recommendations: The optimal landing trajectory and control process obtained in this study align with the recommendations for safe landing after low tail rotor pitch lockup from actual helicopter flight tests. This validates the effectiveness of these strategies and provides a practical guide for pilots facing such situations.

In conclusion, these findings provide valuable insights into how to handle low tail rotor pitch lockups, enhancing the safety and performance of helicopters in such situations. They also contribute to the broader understanding of helicopter control and flight dynamics, which can inform future research and development in this field.

In this study, we simulated two extreme cases of tail rotor pitch lockup: high pitch lockup and low pitch lockup. Typically, conventional tail rotor pitch lockup situations fall between these two extremes. As the next step, we plan to expand our simulations to include more severe conditions such as gusts, turbulence, downdrafts, wind shear, etc., and apply the proposed optimal control method for simulation and optimization, thereby providing feasible control strategies across different flight missions and environments.

6. Conclusion

This paper studies the optimal landing trajectory and control strategy for helicopter encountering different tail rotor pitch lockups using optimal control method. To address this issue, we establish a precise nonlinear flight dynamics model and a pilot model to accurately represent the helicopter dynamics and pilot behavior. The results yield the following conclusions:

(1) High tail rotor pitch lockup typically occurs during high-power flight states such as hovering, low-speed flight, and climbing. As the tail rotor thrust is relatively large, it is recommended to perform a high-power state landing (i.e., keep the engine at high power) with a lower forward speed and descent rate. During landing process, the large lateral force generated by the tail rotor will cause the helicopter to experience significant yaw motion, the pilot can compensate for some of the excess yaw torque by using sideslip.

(2) Low tail rotor pitch lockup typically occurs during low-power flight states such as gliding and level flight near the economic speed. During landing, the pilot can reduce the main rotor collective pitch to decrease the negative torque and balance the heading. This process may result in a relatively large descent rate. For a conventional landing, the small tail rotor thrust cannot balance the high negative torque of the main rotor, leading to a large yaw rate at touchdown, which may cause danger. If an autorotation landing is applied (at a height of about 3 m above the ground), the engine no longer outputs torque to the main rotor, so the landing will be safer with a much lower yaw rate at touchdown.

(3) The optimal control simulation results (landing trajectories and control strategies) are basically consistent with the conclusions of actual flight tests in Refs. [4,5,10]. The landing trajectory and control optimization method for helicopter after tail rotor pitch lockup established in this paper can provide some reference before actual flight test. The findings of this research are expected to provide valuable insights and serve as a reference for subsequent real-time pilot-in-the-loop simulations and final flight tests, contributing to the optimization and refinement of control system design.

In this study, we simulated two extreme cases of tail rotor pitch lockup: high pitch lockup and low pitch lockup. Typically, conventional tail rotor pitch lockup situations fall between these two extremes. However, it should be noted that our current study only considers ideal flight conditions and does not account for the influence of extreme airflow conditions on the landing trajectory and pilot control strategy during tail rotor pitch lockup. As the next step, we plan to expand our simulations to include more severe conditions such as gusts, turbulence, downdrafts, wind shear, etc., and apply the proposed optimal control method for simulation and optimization, thereby providing feasible control strategies across different flight missions and environments.

Currently, this method involves significant computational complexity and cannot be performed in real-time at present. One of our future goals is to achieve real-time computation on the flight control computer based on the current aircraft state.

CRediT authorship contribution statement

Xufei Yan: Investigation, Methodology, Writing – original draft. **Ye Yuan:** Supervision, Validation, Writing – review & editing. **Renliang Chen:** Formal analysis, Project administration, Resources, Supervision.

Declaration of Competing Interest

The authors declare that they have no known competing financial interests or personal relationships that could have appeared to influence the work reported in this paper.

Data availability

No data was used for the research described in the article.

Acknowledgments

None

References

[1] J.H. Saleh, Z. Xu, A.I. Guvir, et al., Data-driven analysis and new findings on the loss of tail rotor effectiveness in helicopter accidents, Sci. Rep. 12 (1) (2022) 2575, https://doi.org/10.1038/s41598-022-06647-0.
[2] A.M. Dequin, The myth of losing tail rotor effectiveness, in: Proceedings of the 45th European Rotorcraft Forum, Warsaw, Poland, 2019, pp. 17–20.
[3] J.H. Saleh, A. Tikayat Ray, K.S. Zhang, et al., Maintenance and inspection as risk factors in helicopter accidents: analysis and recommendations, PLoS One 14 (2) (2019), e0211424, https://doi.org/10.1371/journal.pone.0211424.
[4] J.C. Zhao, Helicopter tail rotor failure analysis and flight test technology research, Aeronaut. Sci. Technol. 26 (3) (2015) 70–73.
[5] Y.O. Arslan, Optimal Trajectory Generation and Tracking for a Helicopter in Tail Rotor Failure, Middle East Technical University, 2022.
[6] A. De Martin, G. Jacazio, A. Nesci, et al., In-depth feature selection for PHM system's feasibility study for helicopters' main and tail rotor actuators, in: Proceedings of the PHM Society European Conference 5, 2020, https://doi.org/10.36001/phme.2020.v5i1.1222, 9-9.

[7] R.H. McSwain, Processing-induced fatigue fracture of a helicopter tail rotor blade, J. Fail. Anal. Prev. (2022) 1–4, https://doi.org/10.31399/asm.fach.v02.c9001298.
[8] A. Mironov, P. Doronkin, The demonstrator of structural health monitoring system of helicopter composite blades, Procedia Struct. Integr. 37 (2022) 241–249, https://doi.org/10.1016/j.prostr.2022.01.080.
[9] P. Zanella, J.V.R. Prasad, C. Johnson, et al., A framework to enhance the mitigation of loss of tail rotor effectiveness, in: Proceedings of the AIAA AVIATION 2022 Forum, 2022, p. 3624, https://doi.org/10.2514/6.2022-3624.
[10] L. Frank, V. Thongsay, US army airworthiness approval for UH-60 Fly-by-wire aircraft flight testing, in: Proceedings of the American Helicopter Society 66th Annual Forum, Arizona, 2010.
[11] X. Yan, R. Chen, S. Zhu, et al., Study of helicopter optimal autorotation landing procedure in tail rotor drive failure, in: Proceedings of the 2022 IEEE International Conference on Robotics and Biomimetics (ROBIO), IEEE, 2022, pp. 668–673, https://doi.org/10.1109/ROBIO55434.2022.10011689.
[12] S. Rajendran, D. Gu, Fault tolerant control of a small helicopter with Tail Rotor Failures in hovering mode, in: Proceedings of the 11th IEEE International Conference on Control & Automation (ICCA), IEEE, 2014, pp. 348–353, https://doi.org/10.1109/ICCA.2014.6870944.
[13] R. Andrea, B.M. Riccardo, S. Pietro, AW169 loss of tail rotor effectiveness simulation, in: Proceedings of the 43rd European Rotorcraft Forum, Forum, Milano, Italy, 2017.
[14] A. Altan, R Hacıoğlu, Model predictive control of three-axis gimbal system mounted on UAV for real-time target tracking under external disturbances, Mech. Syst. Signal Process. 138 (2020), 106548, https://doi.org/10.1016/j.ymssp.2019.106548.
[15] A. Altan, Ö. Aslan, R. Hacıoğlu, Real-time control based on NARX neural network of hexarotor UAV with load transporting system for path tracking, in: Proceedings of the 2018 6th International Conference on Control Engineering & Information Technology (CEIT), IEEE, 2018, pp. 1–6, https://doi.org/10.1109/CEIT.2018.8751829.
[16] A. Altan, Performance of metaheuristic optimization algorithms based on swarm intelligence in attitude and altitude control of unmanned aerial vehicle for path following, in: Proceedings of the 2020 4th International Symposium on Multidisciplinary Studies and Innovative Technologies (ISMSIT), IEEE, 2020, pp. 1–6, https://doi.org/10.1109/ISMSIT50672.2020.9255181.
[17] S. Chashmi, D. Asadi, K. Dastgerdi, Safe land system architecture design of multi-rotors considering engine failure, Int. J. Aeronaut. Astronaut. 3 (1) (2022) 7–19, https://doi.org/10.55212/ijaa.1032693.
[18] H. Haghighi, D. Delahaye, D. Asadi, Performance-based emergency landing trajectory planning applying meta-heuristic and Dubins paths, Appl. Soft Comput. 117 (2022), 108453, https://doi.org/10.1016/j.asoc.2022.108453.
[19] I.R. Lee, Y.S. Choi, M.G. Lim, et al., Guidance and control for autonomous emergency landing of the rotorcraft using the incremental backstepping controller in 3-dimensional terrain environments, Aerosp. Sci. Technol. 132 (2023), 108051, https://doi.org/10.1016/j.ast.2022.108051.
[20] C. Chi, X. Yan, R. Chen, et al., Analysis of low-speed height-velocity diagram of a variable-speed-rotor helicopter in one-engine-failure, Aerosp. Sci. Technol. 91 (2019) 310–320, https://doi.org/10.1016/j.ast.2019.05.003.
[21] X. Yan, R. Chen, S. Zhu, et al., Optimal landing of tilt-rotor aircraft after engine failure considering pilot inherent limitations, in: Proceedings of the 2022 IEEE International Conference on Robotics and Biomimetics (ROBIO), IEEE, 2022, pp. 1036–1040, https://doi.org/10.1109/ROBIO55434.2022.10011647.
[22] Y.U. Zhiming, Y.A.N. Xufei, C. Renliang, Prediction of pilot workload in helicopter landing after one engine failure, Chin. J. Aeronaut. 33 (12) (2020) 3112–3124, https://doi.org/10.1016/j.cja.2020.05.021.
[23] G. Mark, Validation of a Real-Time Engineering Simulation of the UH-60A Helicopter, NASA Ames Research Center, Washington, D C, 1987. Report No. NASA TM-88360.
[24] H. Ji, L. Lu, M.D. White, et al., Advanced pilot modeling for prediction of rotorcraft handling qualities in turbulent wind, Aerosp. Sci. Technol. 123 (2022), 107501, https://doi.org/10.1016/j.ast.2022.107501.
[25] P.A.S.F. Silva, P. Tsoutsanis, A.F. Antoniadis, Numerical investigation of full helicopter with and without the ground effect, Aerosp. Sci. Technol. 122 (2022), 107401, https://doi.org/10.1016/j.ast.2022.107401.
[26] L. Carlo, G. Bottasso, S. Francesco, Trajectory optimization procedures for rotorcraft vehicles including pilot models, with applications to ADS-33 MTEs, Cat-A and engine off landings, in: Proceedings of the American Helicopter Society 65th Annual Forum and Technology Display, AHS, Grapevine, TX, USA, 2009, pp. 1–14, 27–29 May.
[27] R. Veras Neto C, D. de Andrade, Comparison between performance requirements for certification and performance requirements for operation of transport category rotorcraft, J. Aerosp. Technol. Manag. (2022) 14, https://doi.org/10.1590/jatm.v14.1281.
[28] R. Jin, M. Huo, Y. Xu, et al., Rapid cooperative optimization of continuous trajectory for electric sails in multiple formation reconstruction scenarios, Aerosp. Sci. Technol. (2023), 108385, https://doi.org/10.1016/j.ast.2023.108385.
[29] X. Yu, R. Chen, L. Wang, et al., An optimization for alleviating pilot workload during tilt rotor aircraft conversion and reconversion maneuvers, Aerosp. Sci. Technol. 129 (2022), 107854, https://doi.org/10.1016/j.ast.2022.107854.